Inter-comparison of stratospheric mean-meridional circulation and eddy mixing among six reanalysis datasets

K. Miyazaki[1], T. Iwasaki[2], Y.Kawatani[1], C. Kobayashi[3], S. Sugawara[4], M. I. Hegglin[5]

[1]{Japan Agency for Marine-Earth Science and Technology, Yokohama, Japan}

[2]{Department of Geophysics, Graduate School of Science, Tohoku University, Sendai, Japan}

[3]{Meteorological Research Institute, Tsukuba, Japan}

[4]{Department of Science Education, Miyagi University of Education, Sendai, Japan}

[5]{Department of Meteorology, University of Reading, Reading, UK}

Correspondence to: K. Miyazaki (kmiyazaki@jamstec.go.jp)

Abstract

The stratospheric mean-meridional circulation (MMC) and eddy mixing are compared among six meteorological reanalysis datasets: NCEP-NCAR, NCEP-CFSR, ERA-40, ERA-Interim, JRA-25, and JRA-55 for the period 1979–2012. The reanalysis datasets produced using advanced systems (i.e., NCEP-CFSR, ERA-Interim, and JRA-55) generally reveal a weaker MMC and stronger eddy mixing in the Northern Hemisphere (NH) compared with those produced using older systems (i.e., NCEP/NCAR, ERA-40, and JRA-25). In the NH lower stratosphere, the stronger eddy mixing is attributed to stronger planetary-scale mixing in the new datasets, whereas small-scale mixing is weaker in the new datasets. Conventional data assimilation techniques introduce analysis increments without maintaining physical balance, which may have caused an overly strong MMC and spurious small-scale eddies in the old datasets. At the NH mid-latitudes, only ERA-Interim reveals a weakening MMC trend in the deep branch of the Brewer–Dobson circulation (BDC). The relative importance of the eddy mixing compared with the mean transport in the subtropical lower stratosphere is considered to be important in controlling mean Age-of-Air (AoA) variations above, which show increasing trends in ERA-Interim and JRA-55; this together with the weakened MMC in the

deep branch may imply an increasing AoA trend in the NH middle stratosphere in ERA-Interim. Overall, discrepancies between the different variables and trends therein as derived from the different reanalyses are still relatively large, suggesting that more investments into these products are needed in order to obtain a consolidated picture of observed changes in the BDC and the mechanisms that drive them.

1 Introduction

The Brewer–Dobson circulation (BDC), which was discovered by Brewer (1949) and Dobson (1929; 1956), consists of the mean-meridional circulation (MMC) and eddy mixing in the stratosphere. The stratospheric MMC is composed of ascending motions in the tropics, poleward motions toward mid and high latitudes, and descending motions at high latitudes. Planetary waves that propagate from the troposphere break and cause eddy mixing primarily in the stratospheric surf zone surrounding the polar vortex in the winter hemisphere (McIntyre and Palmer, 1983). Because the BDC motion is too slow to measure directly from any measurements, the detailed structure and long-term variations of the BDC have not been well understood.

Stratospheric age-of-air (AoA) (Waugh and Hall, 2002) derived from observation data of long-lived chemical compounds is frequently used as a surrogate for the combined effects of the MMC and eddy mixing in order to investigate the structure and long-term variations in the BDC. Observational studies have found a positive AoA trend in the Northern Hemisphere (NH) mid-latitudes in the middle to upper stratosphere based on balloon measurements of SF_6 and CO_2 for 1975–2005 (Engel et al., 2009), MIPAS SF_6 measurements for 2002–2010 (Stiller et al., 2012), balloon-based measurements of SF_6 and CO_2 for 1975–2012 (Ray et al., 2014), and a merged long-term satellite data record of water vapour for 1986–2010 (Hegglin et al., 2014). In the Southern Hemisphere (SH) mid-latitude lower stratosphere, Stiller et al. (2012) found in contrast a negative AoA trend, a result confirmed by Hegglin et al. (2014). The study by Hegglin et al. (2014) also finds a negative AoA trend in the NH lower stratosphere in contrast to Stiller et al. (2012), with the difference likely explainable by the different time periods considered. However, these observed trends are not fully consistent with simulated results using general circulation models (GCMs), which show instead an acceleration in the mean BDC throughout the stratosphere (e.g., Butchart et al., 2011). The acceleration of the mean BDC strength in the model simulation is associated with enhanced

wave driving (Garcia and Randel, 2008) and shifting critical levels for wave breaking (Shepherd and McLandress, 2011). The reasons for the inconsistency between the measurements and models, especially in the middle and upper stratosphere, have not yet been investigated.

MMC and eddy mixing in the BDC are intrinsically linked (Dunkerton, 1978) and hence play both important roles in determining distributions of long-lived chemical species and AoA in the stratosphere. Interpretation of AoA variations therefore needs to take into account changes in both MMC and eddy mixing. Several recent studies have now quantified the effects of eddy mixing on AoA variations in more detail (Ray et al., 2010; Garny et al., 2014; Ploeger et al., 2015a, 2015b). Garny et al. (2014) stated that eddy mixing causes recirculation of air in the stratosphere, and acts to increase the mean value of AoA. Mixing inside the surf zone modifies the latitudinal distribution of AoA and chemical species, whereas mixing across the subtropical transport barrier is suggested to be important for the mean AoA value above the mixing level (Garny et al., 2014; Ploeger et al., 2015a).

Meteorological reanalyses provide a realistic meteorological field by combining model information with actual observations, and have the potential to provide an alternative tool to study the BDC and AoA variations. Iwasaki et al. (2009) compared four reanalysis datasets (NCEP-NCAR, NCEP-DOE, ERA-40, and JRA-25) and found large differences in their representation of the BDC. Wright and Fueglistaler (2013) showed large differences in the simulated diabatic heat budget in the tropical upper troposphere and lower stratosphere in five reanalysis models (NCEP-NCAR, NCEP-CFSR, JRA-25, ERA-Interim, and MERRA), with substantial implications for representation of transport and mixing. Recently, Abalos et al. (2015) compared the MMC in three reanalyses (ERA-Interim, JRA-55, and MERRA) using three different estimates: from the transformed Eulerian mean (TEM, Andrews and McIntyre, 1976) residual circulation and based on momentum and thermodynamic balances. They showed a relatively large spread (around 40%) among the estimates of the magnitude of tropical upwelling. Monge-Sanz et al. (2007, 2012) highlighted that the representation of the BDC (including eddy mixing) has become much more realistic in ERA-Interim than in ERA-40, thanks to large investments made into improving the reanalysis product. They showed that AoA derived using ERA-Interim displays an increasing trend in the NH mid-latitude stratosphere above 25 km in 1989–2010, consistent with the findings by Hegglin et al. (2014) for 1986–2010. Diallo et al. (2013) showed that the AoA trend derived using ERA-Interim in

the middle stratosphere is positive over the 1989–2010 period. Similarly to what has been accomplished with ERA-Interim, it is important to know whether realistic long-term variations in the BDC have now also been achieved in other reanalysis products.

Differences in the forecast model, assimilated measurements, and data assimilation technique used for producing reanalysis datasets can lead to differences in their representation of the BDC. Model simulations without any assimilation produce meteorological fields that follow the dynamical and thermodynamic balance of the forecast model. Data assimilation analysis increments, introduced by using conventional data assimilation techniques such as the three-dimensional variational (3D-VAR) one, may upset this balance and degrade the expression of momentum budget and wave structures. This is because they introduce an additional force, without maintaining physical balance, as a result of its isotropic and instantaneous analysis increment. In the 3D-VAR analysis, mean ascending motions in the tropics and mixing in the subtropics in the stratosphere were found to be excessively strong (Schoeberl et al., 2003; Tan et al., 2004; Scheele et al., 2005). Advanced data assimilation techniques such as the four-dimensional variational method (4D-VAR) are capable of assimilating observations at the exact time while maintaining the dynamical balance because of the use of flow-dependent analysis, which are expected to improve the representation of both MMC and eddy mixing.

In this paper, we compare MMC and eddy mixing in the stratosphere for six reanalysis datasets; NCEP-NCAR, NCEP-CFSR, ERA-40, ERA-Interim, JRA-25, and JRA-55. The analysis is conducted for the 34 years from 1979 to 2012 based on mass-weighted isentropic zonal means that allow accurate analysis of Lagrangian-mean motions and eddy mixing. Based on the comparison of the mean and eddy components in the BDC, we discuss whether any of the reanalysis data have the potential to reveal useful information on long-term AoA variations.

2 Methodology

2.1 Data

The six reanalysis datasets used in our comparison can be described as follows: 1) NCEP-NCAR – the National Centers for Environmental Prediction (NCEP)-National Center for Atmospheric Research (NCAR) reanalysis product (Kalnay et al., 1996), with a model grid resolution of T62L28 produced using a 3D-VAR technique; 2) NCEP-CFSR – the NCEP Climate Forecast System Reanalysis (Saha et al., 2010) with a model grid resolution of

T382L64 produced using a 3D-VAR technique; 3) ERA-40 – the 40-yr ECMWF Re-Analysis (Simmons and Gibson, 2000) with a model grid resolution of T159L60 produced using a 3D-VAR technique; 4) ERA-Interim – a continuously updated reanalysis since 1979 (Simmons et al., 2007), with a model grid resolution of T225L60 produced using a 4D-VAR technique; 5) JRA-25 – the Japanese 25-year reanalysis product (Onogi et al., 2007), with a model grid resolution of T106L40 provided using a 3D-VAR technique; and 6) JRA-55 – the Japanese 55-year reanalysis product (Kobayashi et al., 2015), with a model grid resolution of T319L60 provided using a 4D-VAR technique.

We here classify NCEP-NCAR, JRA-25, and ERA-40 as old datasets, and NCEP-CFSR, JRA-55, and ERA-Interim as new datasets because of improvements in these latter made by using updated forecast models, updated bias correction algorithms, and advanced data assimilation analysis. We use reanalysis results for the 34 years after 1979, when satellite measurements were assimilated into the reanalysis. For ERA-40, the mean state and linear trend are estimated for the 24 years from 1979 to 2002, since the data are not available after 2002.

2.2 Analysis framework

The analysis of MMC and eddy mixing is based on mass-weighted isentropic zonal means (hereafter referred to as MIM analysis; Iwasaki 1989, 1992; Miyazaki and Iwasaki 2005). The MIM zonal mean is defined as:

$$\overline{A(\phi,\theta,t)}^{*} \equiv \frac{1}{2\pi}\int A(\lambda,\phi,\theta,t)\left(\frac{\partial p}{\partial \theta}\Big/\frac{\partial \overline{p}}{\partial \theta}\right)d\lambda, \quad (1)$$

where ϕ is the latitude, θ is the potential temperature, t is the time, λ is the longitude, and p is the pressure. The asterisks and overbars represent mass-weighting and isentropic zonal means, respectively. Eddies are defined as departures from the mass-weighted zonal means,

$$A' \equiv A - \overline{A^{*}}. \quad (2)$$

Their correlations are given by

$$\overline{\left(A'B'\right)}^{*} = \overline{(AB)}^{*} - \overline{A}^{*}\overline{B}^{*} \quad , (3)$$

We use isentropic zonal mean pressure for the vertical coordinate,

$$p_{\dagger} \equiv \overline{p}_{\dagger} \quad . \quad (4)$$

The log pressure coordinate for isentropic zonal mean pressure is given by

$$z_{\dagger} \equiv -H \log(p_{\dagger} / p_0), \qquad (5)$$

where p_0 = 1000 hPa, $H = g/RT_r$, and p_0, H, g, R and T_r are the reference pressure, scaling height, the acceleration of gravity, gas constant and reference temperature, respectively.

By taking the zonal average on constant isentropes, adiabatic wave motions, which produce Stokes drift, are separated from diabatic effects without having to assume quasigeostrophic flow (Tung, 1982; Andrews 1983; Townsend and Johnson 1985; Iwasaki, 1989, 1992). . Unlike other isentropic coordinate analyses (Andrews, 1983; Tung, 1982, 1986), in the MIM analysis, the mass-weighting is considered not only for meridional circulation but also for other variables such as zonal wind following Johnson (1980). The MIM analysis thus expresses the conservative nature of momentum, heat, and minor constituents, including the exact lower boundary conditions and non-geostrophic effects (Iwasaki, 1989, 1992; Miyazaki and Iwasaki, 2008). The MIM analysis also exactly specifies the eddy diabatic and adiabatic transport terms (Miyazaki and Iwasaki, 2005).

The TEM (Andrews and McIntyre, 1976) provides a useful framework for understanding mean and eddy transports; however, the estimation of the transport fluxes is limited and complicated. Randel et al. (1994), Strahan et al. (1996), and Abalos et al. (2013) estimated eddy transport terms based on eddy flux vectors for small amplitude eddies following Andrews et al. (1987), while some studies estimated this term as residuals considering the uncertainty and difficulty in the eddy transport term estimations (e.g., Randel et al., 1998). The TEM residual circulation represents the difference between the adiabatic temperature changes due to the Eulerian mean vertical velocity $\overline{w}$ and eddy heat flux divergence, in which the quasi-geostrophic approximation and small-amplitude assumption for the Stokes correction are applied and cause disagreement between the TEM residual circulation and Lagrangian mean circulation (Andrews and McIntyre 1976, 1978). For instance, Miyazaki et al. (2008) found a significant (>30%) difference in the mean vertical velocity around the Antarctic polar vortex between the TEM residual vertical velocity and the MIM MMC analysis, which can be attributed to the assumptions applied for the TEM Stokes corrections.

Most of the disadvantages of conventional analysis methods such as TEM (e.g., complicated and inaccurate representation of transport by both mean and eddy motions, lower boundary conditions, and mass conservations) can be avoided using the MIM analysis (Tung, 1986; Iwasaki, 1989; Tanaka et al., 2004; Miyazaki and Iwasaki, 2005).

We here focus on two altitudes; 440 K (at approximately 90–80 hPa) and 560 K (40–30 hPa) as representatives of the shallow and deep branches of the BDC, respectively. Birner and Bönisch (2011) reported that the shallow branch extends to about 50 hPa, and the deep branch is located above that altitude. The analysis results are presented on the isentropic coordinates for diagnosing adiabatic and diabatic transport components. Note that if the potential temperature at a constant pressure changes with time, there would not be exact agreement between the estimated trends in pressure and isentropic coordinates. For example, in the last 30 years (2008–2012 mean minus 1979–1983 mean), potential temperature at 70 hPa decreased by about 2.5 K at low and mid-latitudes in both hemispheres in ERA-Interim. Nevertheless, the general structure of the linear trend was similar between the two coordinates (and hence will not be shown here). The long-term linear trend is estimated based on the least-squares fitting. The statistical significance is determined for the 95% confidence level using the Mann-Kendall test.

2.2.1 Mean-meridional circulation (MMC)

The mass stream function χ in the MIM analysis is calculated from integrating meridional velocity with respect to $p_\dagger$:

$$\chi = a\cos\phi \int_0^{p_\dagger} \overline{v^*}\, dp_\dagger . \quad (6)$$

where a is the Earth's radius, and v is the meridional wind. $\overline{v^*}$ is calculated from meridional wind data with consideration of the mass-weighted isentropic zonal means. Based on the vertical coordinate of the isentropic zonal mean pressure, a diagnostic form the MIM zonal mean continuity equation can be derived:

$$\frac{1}{a\cos\phi}\frac{\partial}{\partial\phi}\left(\overline{v^*}\cos\phi\right) + \frac{1}{\rho_0}\frac{\partial}{\partial z_\dagger}\left(\rho_0 \overline{w^*_\dagger}\right) = 0 , \quad (7)$$

where ρ_0 is the reference atmospheric density. This is valid even when isentropes intersect the ground, by considering the mass-weighted isentropic zonal means of meridional velocities.

The diagnostic form of the zonal mean continuity equation without an eddy term confirms that the mean meridional circulation can be expressed by the nondivergent mass stream function. The mean vertical velocity $\overline{w^*_\dagger}$ is obtained from the mass stream function χ as follows:

$$\overline{w^*_\dagger} = \frac{1}{2\pi a \rho_0 \cos\phi} \frac{\partial \chi}{\partial \phi} \quad . (8)$$

Meanwhile, the local vertical velocity can be estimated as:

$$w_\dagger \equiv \frac{dz_\dagger}{dt} = \left(\frac{\partial z_\dagger}{\partial t} \right)_\theta + \frac{v}{a} \left(\frac{\partial z_\dagger}{\partial \phi} \right)_\theta + \dot{\theta} \frac{\partial z_\dagger}{\partial \theta} . (9)$$

The mass-weighted zonal mean of Eq. (9) gives the relationship between the mean vertical velocity and the diabatic heating as follows:

$$\overline{w_\dagger}^* = \left(\frac{\partial z_\dagger}{\partial t} \right)_\theta + \frac{\overline{v}^*}{a} \left(\frac{\partial z_\dagger}{\partial \varphi} \right)_\theta + \overline{\dot{\theta}}^* \frac{\partial z_\dagger}{\partial \theta} . (10)$$

2.2.2 Eddy mixing

By assuming a flux-gradient linear relationship, the diffusion coefficient provides a measure of eddy mixing. The isentropic diffusion coefficient K_{yy} can be derived from the eddy meridional flux and meridional potential vorticity (PV) gradient on isentropic surfaces (Tung, 1986; Newman et al., 1988; Bartels et al., 1998; Miyazaki and Iwasaki, 2005; Miyazaki et al., 2010b) by neglecting the influence of slant diffusion:

$$\left[\overline{(v'q')}^* \right]_l \approx -K_{yy}(l) \left[\left(\frac{\partial \overline{q}^*}{a \partial \varphi} \right)_\theta \right]_l , (11)$$

where q is the PV, and $[]l$ denotes the time average.

Under frictionless and adiabatic conditions, the PV acts as an atmospheric passive tracer (Hoskins et al., 1985). Miyazaki et al. (2010a) demonstrated that the diabatic source–sink effect on the PV budget is much smaller than the transport effects in the subtropical and extratropical stratosphere. In the K_{yy} estimation, steady conservative wave motions projected

onto a meridional plane can cause apparent diffusion in addition to the true diffusion caused by dissipative wave motions, which may lead to significant differences between the estimated K_{yy} and the true eddy mixing. In our estimates, a time average window t is applied to the eddy PV flux, as in Miyazaki and Iwasaki (2005) and Miyazaki et al. (2010b). This is to reduce the effect of the apparent diffusion effect caused by steady conservative wave motions on K_{yy} and to represent the K_{yy} caused by the true mixing caused by dissipative wave motions. As a result, we expect that the estimated K_{yy} provides information on eddy mixing characteristics similar to estimates of the effective diffusivity (Nakamura, 1996; Haynes and Shuckburgh, 2000).

The absolute value of K_{yy} is influenced by the choice of l (set to one day in this study). In the case of a shorter time window, steady conservative wave motions projected onto the meridional plane cause apparent diffusion in addition to true diffusion. By changing l from 6 hours to 10 days, we confirmed that the estimated K_{yy} becomes smaller with increasing l in all the datasets, but the relative difference of the estimated K_{yy} among the different reanalysis datasets was only slightly influenced by the choice of l. For instance, the 34-year (1979–2012) mean value of K_{yy} (l=*1 day*) averaged over 40–60N from December to February (DJF) at 440 K is smaller than that of K_{yy} (l=*10 days*) by 3.4–6.7% in all the datasets except for ERA-40 (by 0.9% in 1979–2002).

We should note that, even after eliminating the influence of apparent diffusion in K_{yy} estimates, there are limitations in elucidating eddy mixing from these estimates. As discussed by Nakamura (2008), whilst a part of the Eulerian eddy diffusivity (e.g., K_{yy}) can be attributed to instantaneous, irreversible mixing in a way similar to effective diffusivity, the Eulerian eddy diffusivity and eddy diffusivity are fundamentally different, both qualitatively and quantitatively. This is because of difficulties associated with representing eddy advective transport in the Eulerian formulation. Meanwhile, the results of the K_{yy} analysis and related variables are presented here in the geometric latitude coordinate system (where a zonal average is taken for air parcels with different PVs), whereas effective diffusivity is presented in the equivalent latitude (EL) coordinate system (based on the latitude circle that encloses the same area as the PV contour). Latitudinal variations of zonal-mean eddy mixing and associated fields (e.g., strong eddy mixing outside the polar vortex) are more clearly presented in the EL coordinate system.

2.2.3 The relative importance of mean and eddy transports

The zonal mean equation in the MIM analysis can accurately separate meridional transport into mean transport by Lagrangian-mean circulation and eddy (diffusion) transport. In the MIM analysis, the mean and eddy PV fluxes are defined as follows:

$$Mean = \left(\overline{v^*}\,\overline{q^*}, \overline{\dot{\theta}^*}\,\overline{q^*} \right) , \quad (12)$$

$$Eddy = \left(\overline{\left(v'q'\right)^*}, \overline{\left(\dot{\theta}'q'\right)^*} \right) . \quad (13)$$

where $\overline{v^*}$ is calculated from meridional wind data (c.f., Sec. 2.2.1). The diabatic heating $\overline{\dot{\theta}^*}$ can be related to the mean vertical velocity, as described in Eq. (10). The mean transport fluxes are parallel to isopleths of the mass streamfunction, whereas the eddy transport fluxes are parallel to the isentropes under diabatic conditions. Only the meridional components are analyzed in this study.

In order to evaluate the relative importance of eddy transport in each reanalysis product, we estimate the ratio of eddy and total meridional transport fluxes of PV as follows:

$$\frac{\left|\overline{\left(v'q'\right)^*}\right|}{\left|\overline{\left(v'q'\right)^*}\right| + \left|\overline{v^*}\,\overline{q^*}\right|} . \quad (14)$$

If the transport ratio is larger (smaller) than 0.5, the eddy transport (mean transport) dominates the meridional transport on isentropic surfaces.

3 Results

3.1 Eddy mixing

Figure 1 shows the seasonal mean isentropic diffusion coefficient K_{yy} (*l=1 day*) (hereafter referred to as K_{yy}). Large K_{yy} values reveal strong isentropic mixing in the stratospheric surf zone in both hemispheres, but is stronger in the NH than in the SH. The hemispheric asymmetry can be attributed to the differences in planetary wave activity (e.g., Shepherd et al., 2000). The small K_{yy} equatorward of about 30° is indicative of a barrier to horizontal transport between the tropics and mid-latitudes in both hemispheres (Plumb, 1996). At SH high latitudes, K_{yy} becomes large after the break-up of the Antarctic polar vortex (figure not

shown). Strong cross-tropopause eddy mixing is present in the subtropics and mid-latitudes, poleward of the subtropical jet stream, whereas the eddy mixing is strongly suppressed near the core of the subtropical jet stream. These general characteristics are commonly found in all the datasets, and are generally consistent with the analysis of effective diffusivity (e.g., Haynes and Shuckburgh, 2000).

The mean value and linear trend of K_{yy} are estimated in the surf zone (40–60°) and subtropics (15–25°) around the overturning latitude of the MMC (Table 1 and Fig. 2). Isentropic mixing in the surf zone influences the latitudinal gradient of tracers, whereas the mixing across the subtropics is considered to be important for the stratospheric mean AoA because it recirculates old air from the extratropics to the tropics (Garny et al., 2014; Ploeger et al., 2015a). The mean K_{yy} value in the NH surf zone is greater in the new datasets than in the old datasets (about 20% for NCEP, 10% for ERA, and 25% for JRA at 440 K, and about 20% for ERA, and 5% for JRA (not for NCEP) at 560 K). The very large K_{yy} value in NCEP-NCAR in the middle stratosphere is associated with the low top height of the reanalysis product.

The interannual K_{yy} variations both at 440 K and 560 K are remarkably similar among the datasets in the NH mid latitudes during the 34 years considered, and in the SH after 2000 (expect for NCEP-NCAR at 560 K). In the subtropical lower stratosphere, the mean K_{yy} value differs largely among the data products (0.25–0.58 in the NH, and 0.21–0.41 in the SH). The standard deviation in the subtropics is smaller in the new datasets than in the old datasets by 20–30%. The large difference in the subtropical mixing among the datasets could be associated with different representations of the Quasi-biennial oscillation (QBO) in different reanalysis products (Pawson and Fiorino, 1998; Kim and Chun, 2015; Kawatani, personal communication). The shift of the zero wind line associated with the QBO controls propagation ad breaking of planetary waves and leads to large year-to-year variations in the subtropical mixing.

K_{yy} shows an increasing trend in the NH surf zone from the lower to middle stratosphere in all the datasets (+2.1 to +7.5 %/decade in 1979–2012 and +20.7 %/decade in 1979–2001 for ERA-40 at 440 K, and +2.4 to +12.7 %/decade at 560 K). In the SH surf zone, the K_{yy} trend varies largely between the datasets (-2.0 to +16.4 %/decade at 440 K, and -3.0 to +12.5 %/decade at 560 K). The trend in the SH at 560 K is negative only in ERA-Interim. The intensified surf zone mixing could be associated with changes in the critical level. Climate model simulations demonstrated that long-term changes in zonal wind such as the shift of

zero wind line in response to climate change can enhance the upward propagation of westward-propagating waves (Kawatani et al., 2011; Shepherd and McLandress, 2011). Further investigations are required to comprehend the relationship between changes in the critical level, wave forcing, and mixing strength in the reanalysis products.

In the NH subtropical lower stratosphere, K_{yy} shows increasing trends in all datasets except for NCEP-NCAR (+0.3 to +15.5 %/decade), with relatively weak trends in the new datasets (+0.3 to +2.5 %/decade). A large strengthening trend in the subtropical mixing in JRA-25 (+11.6 %/decade) and ERA-40 (+15.5 %/decade) was similarly found in Ray et al. (2010). In the SH subtropical lower stratosphere, the K_{yy} trend is positive only in ERA-Interim (+2.8 %/decade), and shows a large negative value in JRA-25 (-8.5 %/decade) and ERA-40 (-25.5 %/decade). Because of the large interannual variations, the estimated trends are not statistically significant for most cases in the subtropics and the mid-latitudes.

In all the datasets, the K_{yy} trend in the NH surf-zone is positive (+2.5 to +9.7 %/decade) in the first 22 years, then becomes negative (-8.3 to -27.6 %/decade) in the last 12 years (Table 2). The negative trend in the latter period is larger in the new datasets (-21.9 to -27.6 %/decade) than in the old datasets (-8.3 to -16.7 %/decade). These decadal scale changes in the mixing trend seem to be consistent with those in the tropical upward mass flux and MMC in the NH (c.f., Section 3.2). This suggests that variations in wave forcing lead to decadal scale changes in both the mean and eddy transports as is expected, given that these two features are intrinsically connected with each other (c.f., Section 4.1). In the SH surf zone, the positive K_{yy} trend is greater during the last 12 years than during the past 22 years in all the new datasets. In the NH subtropics (not shown in table), K_{yy} shows a greater positive trend in the last 12 years than in the first 22 years in ERA-Interim, whereas the trend is positive in the first 22 years (+4.9 to +14.3 %/decade) and becomes negative in NCEP-CFSR, JRA-25, and JRA-55 in the last 12 years (-9 to -13.4 %/decade).

3.2 Mean-meridional circulation (MMC)

Figure 3 compares the meridional cross section of the mass stream function averaged over DJF and June to August (JJA) in 1979–2012. Note that ERA-40 has been averaged over the shorter time period 1979–2002 due to limited availability of the dataset. Comparison of ERA-40 and ERA-Interim averaged over the same (shorter) time period, however, indicates that the results are comparable. The general structure of the MMC, such as the poleward motion from

low latitudes of the summer hemisphere to mid and high latitudes of the winter hemisphere, and the descending motions at high latitudes of winter hemispheres, is commonly found in all the datasets. However, details regarding the structure, intensity, and trend of the MMC differ among the data. In NCEP-NCAR, the MMC is noisy and unrealistically distorted in the middle stratosphere (altitudes above about 550 K), and also in the SH lower stratosphere during JJA. In ERA-40, it is relatively strong throughout the stratosphere in both hemispheres, as already pointed out by Wohltmann and Rex (2008). Similarly, JRA-25 exhibits an MMC that is somewhat stronger in the middle to upper stratosphere than that found in the other datasets. In NCEP-CFSR, the tropical mean upward motion is distorted in the lower stratosphere, so that mean air trajectories do not ascent in a straight line. Significant diversity of the tropical mean upward motions (not shown) may come from differences in simulated diabatic heating rates in the forecast models (Fueglistaler et al., 2009).

Figure 4 compares the seasonal variation of the mass stream functions at 560 K. The strong mean poleward motions are present from low latitudes to mid and high latitudes from autumn to spring. They are relatively suppressed at the polar vortex edge. In NCEP-NCAR, the cross-equatorial mean-meridional flow is relatively weak throughout the year. Also, the strong poleward flow at mid-latitudes does not exhibit the seasonality apparent in the other reanalyses. In ERA-40 and JRA-25, the mean poleward flow from the subtropics to the mid-latitudes is relatively strong in both hemispheres throughout the year.

The MMC long-term trend differs greatly among the reanalysis datasets (Fig. 5). In NCEP-NCAR, the spatial structure of the linear trend slope is very noisy, likely reflecting inhomogeneities in the reanalysis product. In NCEP-CFSR, the MMC shows a strengthening trend from the tropics to the mid-latitudes in the lower and middle stratosphere in both winter hemispheres. JRA-25 reveals a strengthening trend in the lower and middle stratosphere equatorward of 60N in the NH during winter and throughout the lower stratosphere in the SH in both seasons, whereas it shows a weakening trend above 500 K in the SH in DJF. JRA-55 shows a weak positive trend in the lower stratosphere in winter. ERA-40 reveals a strengthening trend throughout the lower and middle stratosphere over 1979–2002 in the SH in JJA, whereas the trend pattern is noisy in the NH in both seasons. Only in ERA-Interim, the MMC in the NH middle stratosphere (or above about 480 K) tends to weaken during winter. A negative trend is also found from the tropics to the mid-latitudes in both hemispheres in JJA in the middle stratosphere in ERA-Interim. The BDC shallow branch mostly shows a

strengthening trend in ERA-Interim as in other datasets. Abalos et al. (2015) revealed that the acceleration in the MMC is a qualitatively robust result across different estimates (from the TEM residual circulations and based on momentum and thermodynamic balances). Obvious structural changes (i.e., that the shallow and deep branches changed differently) in the wintertime MMC can be found only in ERA-Interim and to some extent also in JRA-25. There are only a few statistically significant estimates in the BDC trends. The low statistical significance could be partly attributed to the fact that large variances associated with ENSO and QBO, as pointed out by Abalos et al. (2015), are not removed in our trend estimates.

Figure 6 compares the time series of the mass stream function at mid-latitudes (40–60°) in the lower stratosphere (440 K) and the middle stratosphere (560 K) during the winter seasons. The mean value and linear trend slope are summarized in Table 3. In the NH mid-latitudes at both altitudes, the mean MMC strength is weaker in the new data than in the old data. At 440 K, NCEP-NCAR was about 60% larger compared to NCEP-CFSR, ERA-40 was 30% larger compared to ERA-Interim, and JRA-25 was 30% larger compared to JRA-55; at 560 K, these values were 40%, 15%, and 30%, respectively. In the NH in DJF, the linear trend slope is positive (indicating a strengthening of the MMC) in all datasets at 440 K (+0.9 to +2.5 %/decade in 1979–2012 and +3.4 %/decade in 1979–2001 for ERA-40) and in all the datasets except for ERA-Interim and ERA-40 at 560 K (+0.9 to +4.0 %/decade). The rate of increase is larger at 440 K than at 560 K in NCEP-CFSR, JRA-25, and JRA-55.

In the SH mid-latitudes in JJA, the mean MMC strength does not reveal any systematic difference between the new and old datasets, whereas the standard deviation (i.e., year-to-year variability) is smaller in the new datasets than in the old datasets by 10–30%. In all the datasets except for ERA-Interim, the MMC tends to strengthen at 440 K; large trends in 1979–2012 are present in NCEP-NCAR, JRA-25, and JRA-55 (-5.4 to -8.4 %/decade). At 560 K, the MMC tends to weaken in ERA-Interim, JRA-25, and NCEP-CFSR (+1.1 to +4.0 %/decade); the largest trend is thereby found in ERA-Interim (+4.0 %/decade). Both the shallow and deep branches of BDC in the SH show strengthening trends in NCEP-NCAR, ERA-40, and JRA-55.

The total upward mass flux was estimated by differencing the maximum and minimum values of the mass stream function along the constant isentropic surfaces (Table 4 and Fig. 7). The annual mean upward mass flux is smaller in the new datasets than in the old datasets (by 8–30% at 440 K and 9–30% at 560 K), as similarly found in the MMC strength in the NH in

DJF. The MMC shows a strengthening trend in all the datasets except for NCEP-NCAR and ERA-Interim at 440 K (+1.4 to +6.0 %/decade in 1979–2012 and +8.5 %/decade in 1979–2001 for ERA-40) and in all datasets except for ERA-Interim at 560 K (+0.6 to +5.3 %/decade). The trend is negative only in ERA-Interim at both altitudes (-3.9 %/decade at 440 K and -6.7 %/decade at 560 K). The estimated trends are statistically significant for the new datasets both at 440 K and 560 K.

Several recent studies have pointed out that AoA and BDC changes occur over timescales of several years to decades (Aschmann et al., 2014; Mahieu et al., 2014; Ray et al., 2014; Poelger et al., 2015b). As summarized in Table 5, the upward mass flux at 440 K shows a strengthening trend during the first 22 years (1979–2000, +1.3 to +9.6 %/decade), but a weakening trend (or slowing strengthening trend) during the last 12 years (2001–2012, -6.3 to +0.9 %/decade) at 440 K in all datasets except for ERA-Interim. ERA-Interim shows a larger negative trend during the last 12 years (-6.0 %/decade) than in the first 22 years (-3.0 %/decade). Abalos et al. (2015) demonstrated that, across nine estimates using three reanalyses (ERA-Interim, JRA-55, and MERRA) and three approaches (derived from the TEM residual circulation and based on momentum and thermodynamic balances), only the residual circulation derived from ERA-Interim shows negative trends in annual mean tropical upwelling. A strong strengthening (weakening) trend is found at 560 K for NCEP-NCAR and JRA-25 (ERA-Interim and JRA-55).

3.3 Wave decomposition

To gain a better understanding of the relative contributions of the wave phenomena on various scales to isentropic mixing, the zonal eddy PV flux is decomposed into individual zonal wavenumber components s using Fast Fourier Transform (FFT) and then normalized by the background meridional PV gradient as follow:

$$K_{yy(s)} = \left(\frac{\left| \left[\overline{v'_s q'_s} \right]_l \right|}{\left[\frac{\partial \overline{q}}{a \partial \varphi} \right]_l} \right)_\theta . \quad (15)$$

The eddy PV flux is separated into three groups: planetary waves (associated with the zonal wavenumbers 1–3), synoptic-scale waves (zonal wavenumbers 4–7), and small-scale waves (zonal wavenumbers 8 and higher).

The relative contribution of these groups is summarized in Table 6. The absolute value of the planetary-scale eddy flux is larger by 10–20% in the new datasets than in the old datasets for all the datasets at 440 K in the NH mid-latitudes, which could be responsible for the stronger mixing in the new datasets. The relative contribution of the planetary-scale mixing to the total eddy flux is also larger in the new datasets in this region, as shown in Table 6. In contrast, the relative contributions of zonal disturbances at synoptic and small scales are somewhat smaller in the new datasets than in the old datasets at 440 K. With conventional data assimilation techniques such as 3D-VAR, physical consistency cannot be maintained during the data assimilation analysis because of lack of flow-dependent background error information, and this probably together with the lower forecast model resolution may cause spurious disturbances and excessive mixing, especially at small scales in the old datasets. For planetary-scale and synoptic-scale waves, forecast model configurations may also be important for the obtained differences (e.g., Biagio et al., 2014).

Each wave group reveals different long-term variations. The planetary-scale disturbance shows increasing trends in the NH surf-zone at both 440 K (+0.3 to +7.2 %/decade in 1979–2012 and +9.4 %/decade in 1979–2001 for ERA-40) and 560 K (+4.4 to +15.2 %/decade in 1979–2012 and +16.9 %/decade in 1979–2001 for ERA-40). At 560 K, all the groups reveal positive trends in all the datasets, with smaller linear trends in the new datasets in most cases.

In the subtropical lower stratosphere (not shown in table), as commonly found in the NH surf zone, the planetary-scale disturbance is stronger, and the small-scale disturbance is weaker in the new datasets than in the old datasets. The positive K_{yy} trend can be mainly attributed to the strengthening trend in the planetary-scale disturbance (+3.1 to +5.2 %/decade) in all datasets except for NCEP-NCAR.

3.4 Relative importance of eddy meridional transport

Atmospheric wave breaking drives both the mean and eddy transports, but in a different manner; it drives the MMC below the breaking level through downward control (Haynes et al., 1991), whereas it causes eddy mixing at the level of wave breaking (e.g., Waugh et al., 1994). Therefore, changes in MMC and eddy mixing do not necessarily occur in the same way in response to changes in atmospheric wave forcing. These wave-induced processes may be represented differently among the reanalysis products.

We compare the relative ratio of the eddy and total meridional PV fluxes (Eq. 14) to investigate the relative importance of these two transport processes. As shown in Fig. 8, the mean meridional transport is dominant equator-ward of about 40° throughout the year, and in the extratropics during the summer. The eddy transport is dominant in the extratropics of the winter hemisphere. Air masses entering the stratosphere are thus dominantly transported by the mean-meridional transport from low to mid-latitudes and then transported mainly by the eddy mixing from the mid- to high latitudes in the winter hemisphere. The strong westerly coincides with the large contribution of the eddy transport. These characteristics are found in a consistent way in all the datasets.

The 34-year mean value of the transport ratio is larger (i.e., the contribution of eddy transport is larger) in the new datasets than in the old datasets both in the extratropics (by 3–8% at 440 K and by about 0–4% at 560 K) and subtropics (by 3–14%) in the NH (Table 7 and Fig. 9). In the NH surf zone, the trend in the transport ratio is different among the datasets, although both the mean and eddy transports showed increasing trends in all the datasets at 440 K and in most datasets except for ERA-40 and ERA-Interim at 560 K. At 560 K, the transport ratio shows a positive trend (i.e., the contribution of the eddy transport becomes more important over time) in the old datasets (+0.3 to +1.5%/decade). The trend is much smaller (or negative) in the new datasets. In the SH surf zone, on the other hand, the trend in the transport ratio varies among the dataset (-4.4 to +2.1 %/decade at 440 K and -3.5 to +1.6 %/decade at 560 K).

In the NH subtropics at 440 K, it is larger in the new datasets (0.25–0.31) than in the old datasets (0.17–0.22), suggesting that eddy-induced recirculation of old air masses from the extratropics to the tropics is more effective than the mean poleward transport of fresh air masses from the tropics into the extratropics in the new datasets, which could have led to older AoA as derived for example in the study by Monge-Sanz et al. (2012), as discussed further in Section 4.2. The transport ratio in the NH subtropics shows a positive trend in most datasets except for NCEP-NCAR and NCEP-CFSR. In the SH subtropics, the trend is negative (the mean transport tends to become more important) in most datasets except for ERA-Interim. The positive trend in ERA-Interim corresponds to the increasing trend in K_{yy} that only appeared in ERA-Interim.

The transport ratio in the NH subtropics reveals a larger positive trend in the last 12 years (+9.9 to +25.5 %/decade) than in the first 22 years (-6 to +3.0 %/decade) in all datasets except for NCEP-CFSR (Table 8). This positive trend implies that the eddy transport has become

more important over time with this tendency becoming even more important during the later time period considered. In the SH subtropics, the mean transport became more important in all datasets except ERA-Interim in the earlier time period, with an increasingly negative trend in the transport ratio for NCEP-NCAR, NCEP-CFSR, and also ERA-Interim in the later time period, along with the mean transport becoming less important in JRA-25 and JRA-55.

4 Discussion

4.1 Dynamical consistency

The relationship between the Eliassen–Palm (E–P) flux divergence and the MMC is expressed through the downward control principle for steady-state conditions. The eddy PV flux in K_{yy} can also be related to the mass flux and E–P flux under the quasi-geostrophic assumption (Andrews et al., 1987; Schneider, 2005). Conventional data assimilation may degrade the wave mean flow and wave mixing relationships. To evaluate the dynamical balance in the reanalysis products, we computed the temporal correlation between the E–P flux divergence and the mass stream function, and between the E–P flux divergence and K_{yy} (l=*1 day*). The E–P flux was estimated based on the MIM zonal mean momentum equation, in which forcings by sub-grid processes were not considered. Momentum changes through sub-grid processes such as gravity wave drag (GWD) parameterization need to be taken into consideration for strict momentum budget analysis. However, these data were not provided in all the datasets, and hence could not be considered in the analysis. The wave-driven adjustment time for the wave mean flow interactions is typically several weeks in the lower stratosphere (Haynes et al., 1991); this effect was also not considered. Instantaneous analysis fields with no time lag were used for the correlation calculation. We here discuss the relationship between the E-P flux divergence at each vertical level and the MMC at 440 K and between the E-P flux divergence at each vertical level and K_{yy} (l=*1 day*) at 560 K. The MMC at 440 K and K_{yy} at 560 K are driven by wave forcings at mostly the same vertical levels (approximately between 500 and 650 K), as discussed below.

As shown in Fig. 10 for ERA-Interim, the mass stream function at 440 K at NH mid-latitudes shows a large correlation with the E–P flux divergence at higher levels, because of downward control. The correlation coefficient averaged between 500 and 650 K at the NH mid-latitudes is larger in the new datasets (approximately 0.5–0.6) than in the old datasets (approximately 0.4) except for JRA (Table 9). This result suggests that the physical balance associated with

the wave mean flow interaction is represented more strictly in the new datasets for the NCEP and ERA datasets. JRA-25 and JRA-55 both reveal large correlation coefficients (approximately 0.6).

K_{yy} (*l=1 day*) at 560 K shows strong correlations with the E–P flux divergence around 500–650 K in ERA-Interim (Fig. 10). This confirms that the reanalysis products represent local wave forcings that drive eddy mixing. There is no systematic difference in the wave-mixing relationship between the new and old datasets. Not only the dynamic balance in analysis increments, but also characteristics of atmospheric diffusivity in the forecast model (e.g., associated with choice of transport scheme and numerical diffusion) could influence the wave-mixing relationship in the reanalysis products.

4.2 Implications for AoA long-term variations

Based on analyses of observational data, several observational studies (e.g., Engel et al., 2009; Stiller et al., 2012; Ray et al., 2014; Hegglin et al., 2014) revealed a positive AoA trend at the NH mid-latitudes from the middle to upper stratosphere, but for different period (1975–2005 in Engel et al. (2009), 2002–2010 in Stiller et al. (2012), 1975–2012 in Ray et al. (2014), and 1986–2010 in Hegglin et al. (2014)). Hegglin et al. (2014) also found a reversed trend in the NH lower stratosphere in 1986–2010.

Using ERA-Interim, Monge-Sanz (2012) and Diallo et al. (2013) have demonstrated an AoA decreasing trend in the NH lower stratosphere and an increasing trend in the middle stratosphere in 1990–2009 and 1989–2010, respectively, consistent with the available observational estimates. As discussed by Garny et al. (2014) and Ploeger et al. (2015a, 2015b), it is essential to take the effects of mixing along the transport pathway into consideration, on top of the effects of the MMC for understanding AoA variations. Interpreting AoA variations simply in terms of changes in the local MMC and eddy mixing effects can be misleading, because the AoA of a given air parcel is the result of the integrated effect of the various tendencies along the parcel trajectory. Although the local analysis given in this study does not allow for the air parcel history and transport pathway variations to be analyzed, it can provide useful information on the general structure of the transport intensity and its potential impacts on AoA variations.

To investigate whether any reanalysis data have the potential to reveal useful implications of long-term AoA variations, we summarize long-term variations in the three important transport

processes: the tropical upward mass flux, the relative contribution of eddy mixing in the subtropics, and the mid-latitudes mean poleward motions ($\overline{v^*}$). We consider that, rather than the mixing strength in the subtropics itself, the relative ratio of the mean and eddy transport is essential to understanding AoA variations, since it determines the ratio of fresh air entering and old air recirculating between the tropics and extratropics. Eddy mixing across the MMC overturning may recirculate old air masses from the extratropics to the tropics, whereas mean poleward flows carry fresh air masses from the tropics to the extratropics, and may return old air masses that were recirculated from the extratropics by eddy transport. Here, we focus on transport processes during winter to explain their possible influences on annual mean AoA variations. In winter, atmospheric waves are active, and strongly induce both MMC and eddy mixing. Abalos et al. (2015) showed that the DJF trends make a major contribution to the overall structure of the annual mean trends of BDC in the NH. However, the influence of transport processes in other seasons cannot be neglected (Konopka et al., 2015). Therefore, the implication obtained from the local analysis of the wintertime transport processes in this study is limited. Explicit calculations of AoA using the reanalysis datasets are required to provide further insights into the role of each transport process on AoA variations.

During the 34 years, from 1979 to 2012, the tropical upward mass flux shows a positive trend from the lower to middle stratosphere, except for ERA-Interim in DJF (consistent with the results of Seviour et al. (2011) and Abalos et al. (2015)), and NCEP-NCAR and ERA-Interim in JJA (Fig. 11). The relative importance of the eddy transport compared to the mean transport shows an increasing trend in ERA-Interim and JRA-55 from the lower to middle stratosphere, which may act to increase AoA, especially in the BDC deep branch. The value of $\overline{v^*}$ at the NH mid-latitudes shows a strengthening trend in the lower stratosphere in most datasets, except for NCEP-CFSR below 440 K. The $\overline{v^*}$ varies largely with height in ERA-Interim, showing a sharp positive trend peak around 400–430 K, and a negative trend above 520 K. To summarize, AoA derived using the reanalysis products in the NH middle stratosphere for the 34 years can be expected to increase in ERA-Interim, and probably also in JRA-55, because of the large increase in the contribution of the eddy mixing in the subtropics and the weakened mean poleward motion in the deep branch. AoA in the NH lower stratosphere can be expected to decrease in all the datasets, except in NCEP-CFSR.

In the SH, the relative importance of the eddy transport to the mean transport in the subtropics shows an increasing trend only in ERA-Interim in the lower stratosphere (above 410 K), and

in ERA-Interim and NCEP-NCAR in the middle stratosphere (above 460 K). The value of $\overline{v^*}$ at the SH mid-latitudes shows a strengthening trend in all the datasets, except for ERA-Interim above 500 K. These changes suggest the possibility of an AoA decreasing trend for both the lower and middle stratosphere in the SH in most datasets except for ERA-Interim during the 34 years. The analysis of ERA-Interim may suggest the possibility of a weaker decreasing or a weak positive AoA trend in the middle stratosphere.

The decadal scale variation in the transport processes will also cause changes in the AoA trend on similar timescales. In the last 12 years (Fig. 12), the upward mass flux trend becomes negative in the lower stratosphere in most datasets, and shows larger increasing trends in the middle stratosphere in all the datasets in DJF. The contribution of the eddy transport in the NH subtropics becomes even more important in the last 12 years in all the datasets, with the largest increase in ERA-Interim. The value of $\overline{v^*}$ at the NH mid-latitudes tends to weaken in most datasets, except for ERA-Interim below 430 K, and all the datasets above that level in the last 12 years. Because of the larger negative trend in $\overline{v^*}$ and the increased contribution of the eddy transport in the subtropics, a larger AoA increasing trend in the NH is expected to be derived using ERA-Interim during the last 12 years than during the 34 years, as suggested by Ploeger et al. (2015b).

In the SH, the relative importance of the eddy transport in the subtropics tends to weaken slightly in most datasets, except for JRA-25 in the last 12 years. JRA-25 reveals substantial decadal scale changes in the transport processes in both hemispheres. ERA-Interim reveals a large decreasing contribution of the eddy transport, which may indicate a significant decreasing trend in AoA in the SH stratosphere in the last 12 years, as consistently revealed by Stiller et al. (2012) for the 2002–2010 period.

4.3 Implications for future developments of reanalyses

Although the reanalysis systems have been individually updated at each operation center, similar aspects were encountered regarding the effects of the system updates on the MMC and eddy mixing, as follows:

1. Both the BDC shallow and deep branches reveal weaker MMC mean intensity (by 15–60% in the NH) and smaller interannual variability (by 10–60% in the SH) in the new

datasets than in the old datasets. This tendency generally will tend to increase AoA throughout the NH stratosphere.

2. Isentropic mixing is stronger in the new datasets than in the old datasets by 10–25%, which can be attributed to stronger planetary-scale mixing in the new datasets in the NH lower stratosphere. In contrast, the contribution of small-scale mixing was smaller in the new datasets, which may be a result of reduced spurious eddies associated with analysis increments using the flow-dependent analysis (but not in NCEP-CFSR) and the use of the higher forecast model resolution.

3. The relative importance of the eddy transport to the mean transport in the NH is larger in the new datasets by up to 8% in the extratropics, and by 3–14% in the subtropics. The larger eddy contribution in the subtropical lower stratosphere may cause an older AoA in the entire stratosphere in the new datasets.

4. The wave mean flow relationship in the NH surf zone is more accurately represented in the new datasets for the NCEP and ERA datasets.

Updated systems can be expected to provide better representations of both the MMC and eddy mixing, because of reduced systematic errors of the forecast model, the application of improved bias correction algorithms, and advanced data assimilation techniques. Nevertheless, it is not straightforward to identify which changes are mainly responsible for the differences in the MMC and eddy mixing.

Monge-Sanz et al. (2007, 2012) investigated that ERA-Interim benefits using an omega-equation balance operator in the background constraint, which is likely to have reduced spurious propagation of eddy motion associated with analysis increments. They also suggested other important factors, such as reduced stratospheric temperature biases of the forecast model and improved bias corrections for satellite radiance data. In ERA-40 and JRA-25, systematic analysis increments were introduced to compensate for model temperature biases, which are thought to cause an overly strong BDC (Uppala et al., 2005). Kobayashi and Iwasaki et al. (2015) found that in JRA-25, the temperature analysis increment evolves from the 1990s to the 2000s, associated with changes in forecast model biases and lack of effective bias corrections, either for the forecast model and assimilated measurements. As a result, the MMC structure in JRA-25 was unrealistically distorted in a particular period corresponding to the changes in external forcing.

The decadal scale variations of the transport processes in the reanalysis could be introduced artificially because of measurement discontinuity. Stratospheric temperatures in ERA-Interim are known to be affected by the introduction of AMSU-A data in 1998 and radio occultation data at the end of 2006 (Dee et al., 2011). Improved bias correction schemes have been implemented in recent reanalysis systems (e.g., variational bias correction in JRA-55 (Kobayashi et al., 2015) and ERA-Interim (Dee and Uppala, 2009)). However, it is still difficult to distinguish between forecast models and measurements biases, and to correct them properly.

In addition, the reanalysis quality could be strongly affected by the performance of the forecast model. Any changes in wave propagation and breaking lead to changes in both the MMC and mixing, but current models have large uncertainties in representing various waves, including forcings from GWD parameterization (e.g., Sigmond and Shepherd, 2014). Further efforts on model development are still important.

5 Conclusions

We compared the characteristics of the stratospheric MMC and eddy mixing in the six reanalysis products for the period 1979–2012 based on mass-weighted isentropic zonal means. Both of the mean and eddy transport processes play important roles in determining distributions and variations of chemical tracers and AoA, thus it is important to clarify whether there are any reanalysis data that can be used to investigate long-term BDC variations.

There were large differences in the MMC strength among the datasets, but there were some similar characteristics. In the NH, the MMC is stronger in the new datasets (NCEP-CFSR, ERA-Interim, and JRA-55) than in the old datasets (NCEP-NCAR, ERA-40, and JRA-25). All the datasets show a strengthening trend in the BDC shallow branch in the winter hemispheres, consistent with model simulations (e.g., Butchart et al., 2010). The MMC in the BDC deep branch showed a weakening trend only in ERA-Interim at the NH mid-latitudes and in ERA-Interim and JRA-25 in the SH mid-latitudes in winter. The vertical structure in the changes as seen in ERA-Interim that would lead to a decrease in AoA in the lower stratosphere and an increase in AoA in the middle (and upper) stratosphere are broadly consistent with inferences made from changes observed in stratospheric water vapour (Hegglin et al., 2014).

Isentropic mixing is generally stronger in the new datasets than in the old datasets, which can be attributed to a stronger large-scale mixing in the new datasets in the lower stratosphere. In

contrast, the contribution of small-scale mixing was smaller in the new datasets, which is considered to be a result of reduced spurious eddies associated with analysis increments in the 4D-VAR analysis. Isentropic mixing shows a strengthening trend in the NH extratropics and subtropics in most cases, associated with strengthened large-scale mixing.

We also evaluated the relative importance of the mean and eddy transports. The contribution of eddy mixing was generally stronger in the new datasets than in the old datasets in the NH. In the subtropical lower stratosphere, the relative contribution of eddy transport showed an increasing trend in datasets, except for NCEP-NCAR and NCEP-CFSR in the NH, and only in ERA-Interim in the SH. These trends reveal changes in the relative effectiveness of eddy-induced recirculation from the extratropics to the tropics, and the mean poleward transport of fresh air into the extratropics; they are considered to be important in understanding AoA variations.

The transport analysis suggests that the ERA-Interim provides a consistent transport picture, with AoA trends derived based on observations in both the deep and shallow branches, whereas other datasets would provide different implications. The increasing trend in AoA in the NH middle stratosphere can be understood as a result of the weakening MMC in the deep branch (found only in ERA-Interim), together with the increased contribution of eddy transport compared with the mean transport in the subtropical lower and middle stratosphere (found in ERA-Interim and JRA-55). The decreasing trend in AoA in the SH lower stratosphere could be a result of the strengthening MMC trends in the shallow branch (large in ERA-Interim and JRA-25). All the reanalysis datasets revealed decadal scale variations in the strength of both MMC and eddy mixing, which may result in significant AoA trend variations. For instance, the increased contribution of the eddy transport in the subtropics and the weakened mean poleward motion in the middle stratosphere during the last 12 years (1979–2000) compared to the first 22 years (2001–2012) in the NH suggests larger increasing trends in AoA in ERA-Interim, NCEP-NCAR, and JRA-55 in the last 12 years.

Differences in data assimilation schemes and forecast models are thought to cause differences in the expression of the MMC and eddy mixing in the BDC among reanalysis products. Our analysis suggests that advanced reanalysis products are potentially useful for studying long-term BDC variations, because of the flow-dependent background error covariance, assimilation of the observations at the exact time, balance operators, and improved bias correction algorithms used in these reanalyses. However, there still seem to be problems that

cause unrealistic atmospheric variations (e.g., large differences in long-term variations between ERA-Interim and JRA-55) associated with discontinuities in the assimilated measurements and large uncertainties in the forecast models. Further efforts are essential to improve the reanalysis systems so that the reanalysis products become more consistent among each other and that they can be used to study the details in BDC variations.

Acknowledgements

We would like to thank Felix Ploeger for his helpful comments on this study. We also would like to thank the two anonymous reviewers for their valuable comments. The work was supported by Grant-in Aid for Scientific Research 15K05296 and 26287117 of MEXT, Japan.

References

Abalos, M., Randel, W. J., Kinnison, D. E., and Serrano, E.: Quantifying tracer transport in the tropical lower stratosphere using WACCM, Atmos. Chem. Phys., 13, 10591-10607, doi:10.5194/acp-13-10591-2013, 2013.

Abalos, M., B. Legras, F. Ploeger and W.J. Randel: Evaluating the advective Brewer-Dobson circulation in three reanalyses for the period 1979-2012. J. Geophys. Res., 120, doi:10.1002/2015JD023182, 2015.

Andrews, D. G., and M. E. McIntyre: Planetary waves in horizontal and vertical shear: The generalized Eliassen–Palm relation and mean zonal acceleration. J. Atmos. Sci., 33, 2031–2048, 1976.

Andrews, D.G. and M.E. McIntyre: An exact theory of nonlinear waves on a Lagrangian-mean flow. J. Fluid. Mech., 89, 609-646, 1978.

Andrews, D.G.: A finite-amplitude Eliassen-Palm theorem in isentropic coordinates. J. Atmos. Sci., 40, 1877-1883, 1983.

Andrews, D. G., J. R. Holton, and C. B. Leovy: Middle Atmosphere Dynamics. Academic Press, Orlando, 489~pp., 1987.

Aschmann, J., Burrows, J. P., Gebhardt, C., Rozanov, A., Hommel, R., Weber, M., and Thompson, A. M.: On the hiatus in the acceleration of tropical upwelling since the beginning of the 21st century, Atmos. Chem. Phys., 14, 12803-12814, doi:10.5194/acp-14-12803-2014, 2014.

Bartels, J., D. Peters, and G. Schmitz: Climatological Ertel's potential-vorticity flux and mean meridional circulation in the extratropical troposphere–lower stratosphere. Ann. Geophys., 16, 250–265, 1998.

Birner, T. and H. Bönisch: Residual circulation trajectories and transit times into the extratropical lowermost stratosphere. Atmos. Chem. Phys., 11, 817–827, 2011.

Biagio, V., S. Calmanti, A. Dell'Aquila, and P. M. Ruti: Northern Hemisphere winter midlatitude atmospheric variability in CMIP5 models, Geophys. Res. Lett., 41, 1277–1282, doi:10.1002/2013GL058928, 2014.

Brewer, A. W.: Evidence for a world circulation provided by measurements of helium and water vapour distribution in the stratosphere, Q. J. R. Meteorol. Soc., 75, 351–363, doi:10.1002/qj.49707532603, 1949.

Butchart, N., Cionni, I., Eyring, V., Shepherd, T. G., Waugh, D. W., Akiyoshi, H., Austin, J., Bru¨hl, C., Chipperfield, M. P., Cordero, E., Dameris, M., Deckert, R., Dhomse, S., Frith, S. M., Garcia, R. R., Gettelman, A., Giorgetta, M. A., Kinnison, D. E., Li, F., Mancini, E., McLandress, C., Pawson, S., Pitari, G., Plummer, D. A., Rozanov, E., Sassi, F., Scinocca, J. F., Shibata, K., Steil, B., and Tian, W.: Chemistry-Climate Model simulations of twenty-first century stratospheric cli- mate and circulation changes, J. Climate, 23, 5349–5374, doi:10.1175/2010JCLI3404.1, 2010.

Dee, D. P. and Uppala, S.: Variational bias correction of satellite radiance data in the ERA-Interim reanalysis, Q. J. Roy. Meteor. Soc., 135, 1830–1841, doi: 10.1002/qj.493, 2009.

Dee, D. P., Uppala, S. M., Simmons, A. J., Berrisford, P., Poli, P., Kobayashi, S., Andrae, U., Balmaseda, M. A., Balsamo, G., Bauer, P. Bechtold, P., Beljaars, A. C. M., van de Berg, L., Bidlot, J., Bormann, N., Delsol, C., Dragani, R., Fuentes, M., Geer, A. J., Haimberger, L., Healy, S. B., Hersbach, H., Ho´lm, E. V., Isaksen, L., Ka˚llberg, P., Ko¨hler, M., Matricardi, M., McNally, A. P., Monge-Sanz, B. M., Morcrette, J.-J., Park, B.- K., Peubey, C., de Rosnay, P., Tavolato, C., The´paut, J.-N., and Vitart, F.: The ERA-Interim reanalysis: configuration and perfor- mance of the data assimilation system, Q. J. Roy. Meteor. Soc., 137, 553–597, doi:10.1002/qj.828, 2011.

Diallo, M., B. Legras, and A. Chedin: Age of stratospheric air in the ERA-Interim, Atmos. Chem. Phys., 12, 12,133–12,154, doi:10.5194/ acp-12-12133-2012, 2012.

Dobson GMB, Harrison DN, Lawrence J.: Measurements of the amount of ozone in the Earth's atmosphere and its relation to other geophysical conditions. Proc. Roy. Soc., Ser. A, 122, 456--486, 1929.

Dobson, G. M. B.: Origin and distribution of polyatomic molecules in the atmosphere, Proc. Roy. Soc., Ser. A, 236, 187, 1956.

Engel, A., Mo¨bius, T., Bo¨nisch, H., Schmidt, U., Heinz, R., Levin, I., Atlas, E., Aoki, S., Nakazawa, T., Sugawara, S., Moore, F., Hurst, D., Elkins, J., Schauffler, S., Andrews, A., and Boering, K.: Age of stratospheric air unchanged within un- certainties over the past 30 years, Nature Geosci., 2, 28–31, doi:10.1038/ngeo388, 2009.

Fueglistaler, S., Legras, B., Beljaars, A., Morcrette, J.-J., Sim- mons, A., Tompkins, A. M., and Uppala, S.: The diabatic heat budget of the upper troposphere and lower/mid stratosphere in ECMWF reanalyses, Q. J. Roy. Meteor. Soc., 135, 21–37, doi:10.1002/qj.361, 2009.

Garcia, R. R. and Randel, W. J.: Acceleration of Brewer-Dobson circulation due to the increases in greenhourse gases, J. Atmos. Sci., 65, 2731–2739, doi:10.1175/2008JAS2712.1, 2008.

Garny, H., T. Birner, H. Bönisch, and F. Bunzel: The effects of mixing on age of air, J. Geophys. Res., 119, 7015–7034, doi:10.1002/2013JD021417, 2014.

Haynes, P., and E. Shuckburgh: Effective diffusivity as a diagnostic of atmospheric transport: 1. Stratosphere, J. Geophys. Res., 105, 22777–22794, doi:10.1029/2000JD900093, 2000.

Haynes, P., C. J. Marks, M. E. McIntyre, T. G. Shepherd, and K. P. Shine: On the ‘‘downward control’’ of extratropical diabatic circulations by eddy-induced mean zonal forces, J. Atmos. Sci., 48, 651–678, 1991.

Hegglin, M. I., D. Plummer, J. Scinocca, T. G. Shepherd, J. Anderson, L. Froidevaux, B. Funke, D. Hurst, A. Rozanov, J. Urban, T. v. Clarmann, K. A. Walker, R. Wang, S. Tegtmeier, and K. Weigel, Variation of stratospheric water vapour trends with altitude from merged satellite data, *Nat. Geosci.*, 7, 768--776, doi: 10.1038/NGEO2236, 2014.

Hoskins, B. J., M. E. McIntyre, and A. W. Robertson: On the use and significance of isentropic potential vorticity maps, Quart. J. Roy. Meteor. Soc., 111, 877–946, 1985.

Iwasaki, T.: A diagnostic formulation for wave–mean flow interactions and Lagrangian-mean circulation with a hybrid vertical coordinate of pressure and isentropes, J. Meteor. Soc. Japan, 67, 293–312, 1989.

Iwasaki, T.: General circulation diagnosis in the pressure-isentrope hybrid vertical coordinate. *J. Meteor. Soc. Japan,* 70, 673–687, 1992.

Iwasaki, T., Hamada, H., and Miyazaki, K.: Comparisons of Brewer-Dobson circulations diagnosed from reanalyses, J. Meteorol. Soc. Japan, 87, 997–1006, doi:10.2151/jmsj.87.997, 2009.

Johnson, D.R.: A Generalized Transport Equation for Use with Meteorological Coordinate Systems. Mon. Wea. Rev., 108, 733–745, 1980.

Kalnay, E., M. Kanamitsu, R. Kistler, W. Collins, D. Deaven, L. Gandin, M. Iredell, S. Saha, G. White, J. Woollen, Y. Zhu, A. Leetmaa, R. Reynolds, M. Chelliah, W. Ebisuzaki, W. Higgins, J. Janowiak, K. C. Mo, C. Ropelewski, J. Wang, R. Jenne, D. Joseph: The NCEP/NCAR 40-Year Reanalysis Project, Bull. Am. Meteor. Soc., 77, 437–472, 1996.

Kim, Y.-H. and Chun, H.-Y.: Momentum forcing of the quasi-biennial oscillation by equatorial waves in recent reanalyses, Atmos. Chem. Phys., 15, 6577-6587, doi:10.5194/acp-15-6577-2015, 2015.

Kobayashi, S., Y. Ota, Y. Harada, A. Ebita, M. Moriya, H. Onoda, K. Onogi, H. Kamahori, C. Kobayashi, H. Endo, K. Miyaoka, and K. Takahashi: The JRA-55 Reanalysis: General Specifications and Basic Characteristics, J. Meteor. Soc. Japan, 93, 5–48, doi:10.2151/jmsj.2015-001, 2015.

Kobayashi, C. and T, Iwasaki, Brewer-Dobson circulation diagnosed from JRA-55, J. Geophys. Res., revised, 2015.

Konopka, P., Ploeger, F., Tao, M., Birner, T. and Riese, M.: Hemispheric asymmetries and seasonality of mean age of air in the lower stratosphere: Deep versus shallow branch of the Brewer-Dobson circulation, J. Geophys. Res., 120, 2053–2066. doi: 10.1002/2014JD022429, 2015.

Lyjak, L. V., and V. A. Yudin: Diagnostics of the large-scale mixing properties from stratospheric analyses, J. Geophys. Res., 110, D17107, doi:10.1029/2004JD005577, 2005.

Mahieu, E., Chipperfield, M. P., Notholt, J., Reddmann, T., Anderson, J., Bernath, P. F., Blumenstock, T., Coffey, M. T., Dhomse, S. S., Feng, W., Franco, B., Froidevaux, L., Griffith, D. W. T., Hannigan, J. W., Hase, F., Hossaini, R., Jones, N. B., Morino, I., Murata, I., Nakajima, H., Palm, M., Paton-Walsh, C., Russell III, J. M., Schneider, M., Servais, C., Smale, D. & Walker, K. A.: Recent Northern Hemisphere stratospheric HCl increase due to atmospheric circulation changes, Nature, 515, 104–107, 2014.

McIntyre, M. E., and T. N. Palmer: Breaking planetary waves in the stratosphere, Nature, 305, 593–600, doi:10.1038/305593a0, 1983.

Miyazaki, K., and T. Iwasaki: Diagnosis of meridional ozone transport based on mass-weighted isentropic zonal means, J. Atmos. Sci., 63, 1192–1208, 2005.

Miyazaki, K., and T. Iwasaki: The gradient genesis of stratospheric trace species in the subtropics and around the polar vortex, J. Atmos. Sci., 65, 490–508, 2008.

Miyazaki, K., S. Watanabe, Y. Kawatani, Y. Tomikawa, M. Takahashi, and K. Sato: Transport and mixing in the extratropical tropopause region in a high-vertical-resolution GCM. Part I: Potential vorticity and heat budget analysis, J. Atmos. Sci., 67, 1293–1314, 2010a.

Miyazaki, K., Sato, S. Watanabe, Y. Tomikawa, Y. Kawatani, and M. Takahashi: Transport and mixing in the extratropical tropopause region in a high-vertical-resolution GCM. Part II: Importance of small-scale disturbances, J. Atmos. Sci., 67, 1315–1336, 2010b.

Monge-Sanz, B. M., Chipperfield, M. P., Simmons, A. J., and Uppala, S. M.: Mean age of air and transport in a CTM: comparison of different ECMWF analyses, Geophys. Res. Lett., 340, L04801, doi:10.1029/2006GL028515, 2007.

Monge-Sanz, B. M., Chipperfield, M. P., Dee, D. P., Simmons, A. J., and Uppala, S. M.: Improvements in the stratospheric transport achieved by a chemistry transport model with ECMWF (re)analyses: identifying effects and remaining challenges, Q. J. R. Meteorol. Soc., 139, 654--673, doi:10.1002/qj.1996, 2012.

Nakamura, N.: Two-dimensional mixing, edge formation, and permeability diagnosed in area coordinates, J. Atmos. Sci., 53, 1524–1537, 1996.

Nakamura, N.: Quantifying inhomogeneous, instantaneous, irreversible transport using passive tracer field as a coordinate. Transport and Mixing in Geophysical Flows, J. B. Weiss and A. Provenzale, Eds., Lecture Notes in Physics, Vol. 744, Springer-Verlag, 137–164, 2008

Newman, P. A., M. R. Schoeberl, R. A. Plumb, and J. E. Rosenfield: Mixing rates calculated from potential vorticity, J. Geophys. Res., 93, 5221–5240, 1988.

Onogi, K., J. Tsutsui, H. Koide, M. Sakamoto, S. Kobayashi, H. Hatsushika, T. Matsumoto, N. Yamazaki, H. Kamahori, K. Takahashi, S. Kadokura, K. Wada, K. Kato, R. Oyama, T. Ose, N. Mannoji and R. Taira: The JRA-25 Reanalysis, J. Meteor. Soc. Japan, 85, 369–432, doi:10.2151/jmsj.85.369, 2007.

Pawson, S., and M. Fiorino: A comparison of reanalyses in the lower tropical stratosphere: Part 2. The quasi-biennial oscillation, Clim. Dyn., 14, 645–658, 1998.

Ploeger, F., M. Abalos, T. Birner, P. Konopka, B. Legras, R. Müller, and M. Riese: Quantifying the effects of mixing and residual circulation on trends of stratospheric mean age of air. Geophys. Res. Lett., 42, 2047–2054. doi: 10.1002/2014GL062927, 2015a.

Ploeger, F., M. Riese, F. Haenel, P. Konopka, R. Müller, and G. Stiller: Variability of stratospheric mean age of air and of the local effects of residual circulation and eddy mixing, J. Geophys. Res., 120, 716–733, doi:10.1002/2014JD022468, 2015b.

Plumb, R. A., A ‘‘tropical pipe’’ model of stratospheric transport, J. Geophys. Res., 101, 3957–3972, 1996.

Randel, W. J., R. Garcia, and F. Wu: Dynamical balances and tropical stratospheric upwelling, J. Atmos. Sci., 65, 3584–3595, doi:10.1175/2008JAS2756.1, 2008.

Ray, E. A., Moore, F. L., Rosenlof, K. H., Davis, S. M., Boenisch, H., Morgenstern, O., Smale, D., Rozanov, E., Hegglin, M., Pitari, G., Mancini, E., Braesicke, P., Butchart, N., Hardiman, S., Li, F., Shibata, K., and Plummer, D. A.: Evidence for changes in stratospheric transport and mixing over the past three decades based on multiple data sets and tropical leaky pipe analysis, J. Geophys. Res., 115, D21304, doi:10.1029/2010JD014206, 2010.

Ray, E. A., F. L. Moore, K. H. Rosenlof, S. M. Davis, C. Sweeney, P. Tans, T. Wang, J. W. Elkins, H. Boenisch, A. Engel, S. Sugawara, T. Nakazawa, and S. Aoki: Improving stratospheric transport trend analysis based on SF_6 and CO_2 measurements, J. Geophys. Res., 119, 14,110–14,128, doi:10.1002/2014JD021802, 2014.

Saha, S., Moorthi, S., Wu, X., Wang, J., Nadiga, S., Tripp, P., Behringer, D., Hou, Y.-T., Chuang, H.-Y., Iredell, M., Ek, M., Meng, J., Yang, R., Peoa, M., van den Dool, M., Zhang, Q., Wang, W., Chen, M., and Becker, M.: The NCEP climate forecast system version~2, J. Climate, 27, 2185–2208, 2013.

Scheele, M. P., Siegmund, P. C., and Velthoven, P. F. J.: Stratospheric age of air computed with trajectories based on various 3D-Var and 4D-Var data sets, Atmos. Chem. Phys., 5, 1–7, doi:10.5194/acp-5-1-2005, 2005.

Schneider, T.: Zonal momentum balance, potential vorticity dynamics, and mass fluxes on near-surface isentropes, J. Atmos. Sci., 62, 1884–1900, 2005.

Schoeberl, M. R., Douglass, A. R., Zhu, Z., and Pawson, S.: A comparison of the lower stratospheric age spectra derived from a general circulation model and two data assimilation systems, J. Geophys. Res., 108, 4113, doi:10.1029/2002JD002652, 2003.

Seviour, W. J. M., Butchart, N., and Hardiman, S. C.: The Brewer-Dobson circulation inferred from ERA-Interim, Q. J. Roy. Meteor. Soc., 138, 878–888, doi:10.1002/qj.966, 2011.

Shepherd, T. G.: The middle atmosphere, J. Atmos. Solar-Terr. Phys., 62, 1587-1601, doi: 10.1016/S1364-6826(00)00114-0, 2000.

Shepherd T. G., McLandress, C.: A robust mechanism for strengthening of the Brewer–Dobson circulation in response to climate change: Critical-layer control of subtropical wave breaking, J. Atmos. Sci., 68, 784–797, 2011.

Sigmond, M., T. Shepherd: Compensation between Resolved Wave Driving and Parameterized Orographic Gravity Wave Driving of the Brewer–Dobson Circulation and Its Response to Climate Change, J. Climate, 27, 5601–5610, 2014.

Simmons, A., Uppala, S., Dee, D., Kobayashi, S.: ERA-Interim: New ECMWF reanalysis products from 1989 onwards, ECMWF newsletter, 110, 25–35, 2007.

Stiller, G. P., von Clarmann, T., Haenel, F., Funke, B., Glatthor, N., Grabowski, U., Kellmann, S., Kiefer, M., Linden, A., Lossow, S., and López-Puertas, M.: Observed temporal evolution of global mean age of stratospheric air for the 2002 to 2010 period, Atmos. Chem. Phys., 12, 3311–3331, doi:10.5194/acp-12-3311- 2012, 2012.

Tan, W., M. A. Geller, S. Pawson, and A. M. da Silva: A case study of excessive subtropical transport in the stratosphere of a data assimilation system, J. Geophys. Res., 109, D11102, doi:10.1029/2003JD004057, 2004.

Tanaka, D., T. Iwasaki, S. Uno, M. Ujiie and K. Miyazaki, Eliassen-Palm flux diagnosis based on isentropic representation, J. Atmos. Sci., 61 2370-2383, 2004.

Townsend R.D. and D.R. Johnson: A diagnostic study of the isentropic tonally averaged mass circulation during the first CARP global experiment. J. Atmos. Sci., 42, 1565-1579, 1985.

Tung, K.K.: On the two dimensional transport of stratospheric trace gases in isentropic coordinates. J. Atmos. Sci., 39, 2330-2355, 1982.

Tung, K.K.: On the relationship between the thermal structure of the stratosphere and the seasonal distribution of ozone, Geophys. Res. Lett., 13, 1308–1311, doi: 10.1029/GL013i012p01308, 1986.

Waugh, D., R. A. Plumb, R. J. Atkinson, M. R. Schoeberl, L. R. Lait, P. Newman, M. Loewenstein, D. Toohey, L. Avallone, C. R. Webster, and R. May: Transport out of the lower stratospheric Arctic vortex by Rossby wave breaking, J. Geophys. Res., 99, 1071–1088, doi:10.1029/93JD02556, 1994.

Waugh, D.W., and T.M. Hall: Age of stratospheric air: Theory, observations, and models, Rev. Geophys. , 40, 4, doi:10.1029/2000RG000101, 2002.

Wohltmann, I. and Rex, M.: Improvement of vertical and residual velocities in pressure or hybrid sigma-pressure coordinates in analysis data in the stratosphere, Atmos. Chem. Phys., 8, 265-272, doi:10.5194/acp-8-265-2008, 2008.

Wright, J. S. and Fueglistaler, S.: Large differences in reanalyses of diabatic heating in the tropical upper troposphere and lower stratosphere, Atmos. Chem. Phys., 13, 9565-9576, doi:10.5194/acp-13-9565-2013, 2013.

Uppala, S., Kallberg, P., Simmons, A., Andrae, U., da Costa Bechtold, V., Fiorino, M., Gibson, J., Haseler, J., Hernandez, A., Kelly, G., Li, X., Onogi, K., Saarinen, S., Sokka, N., Allan, R., Andersson, E., Arpe, K., Balmaseda, M., Beljaars, A., van de Berg, L., Bidlot, J., Bormann, N., Caires, S., Chevallier, F., Dethof, A., Dragosavac, M., Fisher, M., Fuentes, M., Hagemann, S., Holm, E., Hoskins, B., Isaksen, L., Janssen, P., Jenne, R., McNally, A., Mahfouf, J.-F., Morcrette, J.-J., Rayner, N., Saunders, R., Simon, P., Sterl, A., Trenberth, K., Untch, A., Vasiljevic, D., Viterbo, P., and Woollen, J.: The ERA-40 re-analysis, Q. J. Roy. Meteor. Soc., 131, 2961–3012, doi:10.1256/qj.04.176, 2005.

Table 1. Mean value over 34 years (1979–2012) of K_{yy} (*l=1 day*) (in 10^6 m^2/s) averaged over 40–60N at 440 K and 560 K and over 15–25N at 440 K in DJF, and averaged over 40–60S at 440 K and 560 K and over 15–25S at 440 K in JJA. The linear trend slope (in %/decade ± standard deviation) is also shown in brackets. The linear trend with a confidence level greater than 95% is shown in bold.

	NCEP-NCAR	NCEP-CFSR	ERA-40	ERA-Interim	JRA-25	JRA-55
40N–60N 440K	2.89 (+7.3±16.9)	3.47 (+3.8±15.5)	3.07 (+20.7±14.5)	3.37 (+7.5±17.4)	2.93 (+2.1±15.7)	3.69 (+4.5±16.0)
40N–60N 560K	6.89 (+2.4±9.7)	3.53 (+10.7±27.6)	3.14 (+11.3±24.8)	3.7 (+11.0±27.6)	3.49 (+12.7±28.0)	3.68 (+11.7±28.2)
15N–25N 440K	0.25 (-6.3±12.2)	0.58 (+0.3±13.0)	0.48 (+15.5±17.9)	0.42 (+1.7±6.9)	0.40 (**+11.6±12.4**)	0.48 (+2.5±8.7)
40S–60S 440K	0.70 (-1.7±13.0)	0.83 (-2.0±13.4)	0.90 (+16.4±12.3)	0.74 (+1.6±14.1)	0.71 **(+15.8±14.9)**	0.74 (+4.2±14.8)
40S–60S 560K	3.14 (**+12.5±12.2**)	0.5 (+4.1±17.3)	0.25 (+8.7±58.9)	0.62 (-3.0±14.3)	0.41 (+10.4±26.0)	0.52 (+0.7±18.5)
15S–25S 440K	0.34 (-0.7±7.0)	0.33 (-3.0±9.2)	0.21 (-25.5±15.3)	0.27 (+2.8±6.9)	0.41 (**-8.5±10.0**)	0.31 (-0.9±7.9)

Table 2. Linear trend slope of K_{yy} (*l=1 day*) (in %/decade) for 40N–60N in DJF and for 40S–60S in JJA at 560 K during the first 22 years (1979–2000) and during the last 12 years (2001–2012).

	NCEP-NCAR	NCEP-CFSR	ERA-40	ERA-Interim	JRA-25	JRA-55
40N–60N 560K (1979–2000)	+9.7	+5.6	+4.0	+2.5	+4.9	+2.6
40N–60N 560K (2001–2012)	-8.3	-27.6		-23.8	-16.7	-21.9
40S–60S 560K (1979–2000)	+16.1	+1.5	-2.6	+4.2	+20.2	+2.3
40S–60S 560K (2001–2012)	+12.1	+15.6		+11.9	+18.9	+13.8

Table 3. Same as in Table 1, but for the mass stream function (in 10^{10} kg/s) averaged over 40–60N in DJF, and over 40–60S in JJA at 440 K and 560 K. The linear trend slope (in %/decade ± standard deviation) is also shown in brackets. The linear trend with a confidence level greater than 95% is shown in bold.

	NCEP-NCAR	NCEP-CFSR	ERA-40	ERA-Interim	JRA-25	JRA-55
40N–60N 440K	0.71 (+2.1±4.3)	0.45 (+1.9±5.6)	0.56 (+3.4±6.5)	0.44 (+1.8±5.4)	0.61 (+0.9±3.9)	0.48 (+2.5±4.5)
40N–60N 560K	0.40 (+0.9±5.1)	0.28 (+2.2±5.4)	0.31 (-2.0±6.6)	0.27 (-3.3±4.9)	0.36 (+1.3±4.7)	0.28 (+**4.0**±**5.0**)
40S–60S 440K	-0.28 (-5.4±9.4)	-0.22 (-0.7±8.3)	-0.20 (-22.3±9.1)	-0.18 (+0.1±8.2)	-0.23 (**-8.4**±**7.2**)	-0.25 (**-6.7**±**4.9**)
40S–60S 560K	-0.16 (-6.4±13.0)	-0.13 (+2.0±9.5)	-0.10 (-18.2±9.0)	-0.09 (+4.0±3.5)	-0.14 (+1.1±9.7)	0.14 (-4.1±7.4)

Table 4. Same as in Table 1, but for the annual mean total upward flux (in 10^{10} kg/s) and its linear trend slope (in %/decade ± standard deviation in brackets) at 440 K and 560 K.

	NCEP-NCAR	NCEP-CFSR	ERA-40	ERA-Interim	JRA-25	JRA-55
440K	0.98 (-1.8±2.7)	0.67 (**+6.0±3.3**)	0.89 (+8.5±4.7)	0.73 (**-3.9±2.2**)	0.86 (**+1.4±1.8**)	0.795 (**+1.7±1.3**)
560K	0.48 (+2.1±4.3)	0.34 (**+5.3±4.8**)	0.47 (+2.3±3.4)	0.36 (**-6.7±3.2**)	0.44 (+0.6±3.4)	0.40 (**+2.1±1.9**)

Table 5. Linear trend of the annual mean tropical total mean upward flux (in %/decade) during the first 22 years (1979–2000), and during the last 12 years (2001–2012) at 440 K and 560 K.

	NCEP-NCAR	NCEP-CFSR	ERA-40	ERA-Interim	JRA-25	JRA-55
1979–2000 440K	+1.3	**+9.6**	+9.3	-3.0	**+3.8**	**2.7**
2001–2012 440K	-6.3	-2.0		-6.0	+0.9	-1.6
1979–2000 560K	+1.2	**+9.9**	+3.5	-4.1	+2.1	+2.8
2001–2012 560K	+8.1	+5.9		-10.1	+20.0	-3.2

Table 6. Relative contribution of different wave components to zonal eddy PV component (in %) and the linear trend slope (in %/decade in brackets) averaged over 40–60N at 440 K and 560 K in DJF in 1979–2012.

		NCEP-NCAR	NCEP-CFSR	ERA-40	ERA-Interim	JRA-25	JRA-55
40N–60N 440K	1-3	52.4 (+2.2)	56.1 (+7.2)	54.8 (+9.4)	56.1 (+0.3)	54.7 (+3.0)	56.1 (+4.2)
	4-7	36.6 (-1.8)	35.3 (+4.8)	36.4 (-0.9)	35.6 (-1.1)	36.5 (-0.4)	35.7 (+1.9)
	8-	11.0 (-1.6)	8.5 (+3.8)	8.8 (+16.7)	8.4 (+1.4)	8.8 (+2.6)	8.2 (+7.1)
40N–60N 560K	1-3	69.4 (+15.2)	71.6 (+4.8)	71.8 (+16.9)	70.8 (+4.4)	72.7 (+7.7)	72.1 (+4.8)
	4-7	23.7 (+12.2)	24.2 (+4.3)	23.8 (+13.2)	24.8 (+7.4)	23.5 (+10.2)	23.9 (+3.3)
	8-	6.9 (+14.3)	4.2 (+1.5)	4.4 (+16.7)	4.4 (+4.2)	3.7 (+13.1)	4.0 (+15.4)

Table 7. Same as in Table 1, but for the relative importance of the eddy transport to the total meridional transport averaged over 40–60N at 440 and 560 K and 15–25N at 440 K in DJF, and over 40–60S at 440 K and 560 K and 15S–25S at 440K in JJA, and its linear trend slope (in %/decade ± standard deviation in brackets).

	NCEP-NCAR	NCEP-CFSR	ERA-40	ERA-Interim	JRA-25	JRA-55
40N–60N 440K	0.48 (-0.5±2.7)	0.56 (+1.0±2.5)	0.50 (+0.0±3.4)	0.57 (-0.1±2.5)	0.52 (+0.5±3.5)	0.55 (+1.1±2.7)
40N–60N 560K	0.53 (+1.5±2.8)	0.53 (+0.1±2.8)	0.50 (+0.9±2.7)	0.54 (-0.1±2.9)	0.48 (+0.3±3.0)	0.52 (-0.1±2.8)
15N–25N 440K	0.17 (-1.4±7.1)	0.31 (-3.1±5.3)	0.18 (+0.5±9.1)	0.26 (+3.1±6.5)	0.22 (+7.2±8.1)	0.25 (+3.9±5.2)
40S–60S 440K	0.55 **(-1.5±1.5)**	0.54 (+0.0±1.6)	0.53 (+2.1±2.0)	0.53 (+0.3±1.6)	0.58 **(-4.4±3.1)**	0.54 (-0.5±1.6)
40S–60S 560K	0.60 (+1.6±2.4)	0.55 (+0.7±2.5)	0.57 (-3.5±3.2)	0.57 (+0.5±2.5)	0.57 (-1.1±2.9)	0.54 (-1.3±2.7)
15S–25S 440K	0.28 (-2.3±4.8)	0.32 **(-5.2±4.0)**	0.22 (-18.4±13.1)	0.27 (+3.3±6.0)	0.41 **(-12.9±5.6)**	0.25 **(-5.4±4.2)**

Table 8. Linear trend slope of the relative importance of the eddy transport to the total meridional transport (in %/decade) for 15N–25N in DJF, and for 15S–25S in JJA at 440 K during the first 22 years (1979–2000), and during the last 12 years (2001–2012).

	NCEP-NCAR	NCEP-CFSR	ERA-40	ERA-Interim	JRA-25	JRA-55
15N-25N 440K (1979-2000)	-6.0	3.0	0.3	1.6	3.0	1.7
15N-25N 440K (2001-2012)	23.2	-2.7		25.5	9.9	10.4
15S-25S 440K (1979-2000)	-0.9	-2.9	-19.4	5.0	**-18.7**	**-11.7**
15S-25S 440K (2001-2012)	-11.6	-5.2		-7.9	21.6	-5.2

Table 9. Correlation coefficient between the mass stream function (Mean) at 50N, 440 K, and the E–P flux divergence at each grid point averaged between 500 and 650 hPa and 50N-60N, and between K_{yy} (*l=1 day*) at 50N, 560 K, and the E–P flux divergence at each grid point averaged between 550 and 650 hPa and 45N-55N in DJF in 2001–2012 (1990–2001 for ERA-40).

	NCEP-NCAR	NCEP-CFSR	ERA-40	ERA-Interim	JRA-25	JRA-55
Mean	-0.42	-0.61	-0.39	-0.58	-0.61	-0.59
K_{yy} *(l=1 day)*	-0.16	-0.36	-0.46	-0.35	-0.35	-0.35

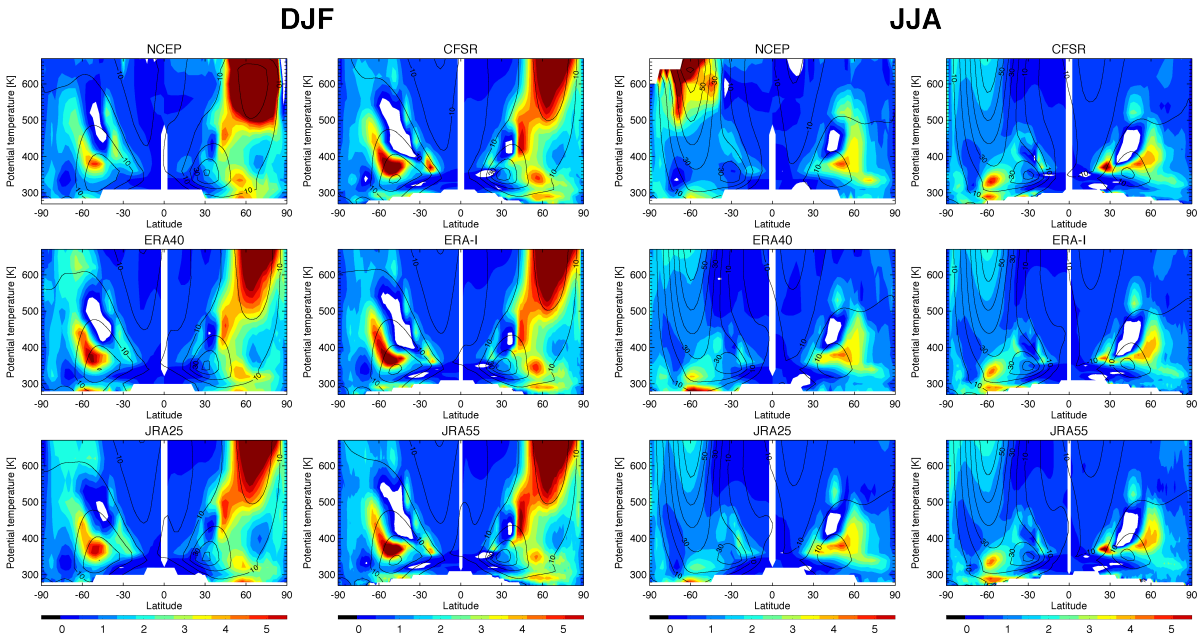

Figure 1. Latitude and potential temperature cross section of the isentropic diffusion coefficient Kyy (in 10^6 m^2/s) averaged for December to February (DJF, left panel) and June to August (JJA, right panel) over the time period 1979–2012 (1979–2002 for ERA-40,). The results are shown for the NCEP-NCAR reanalysis (top left), NCEP-CFSR (top right), ERA-40 (middle left), ERA-Interim (middle right), JRA-25 (bottom left), and JRA-55 (bottom right) in each panel.

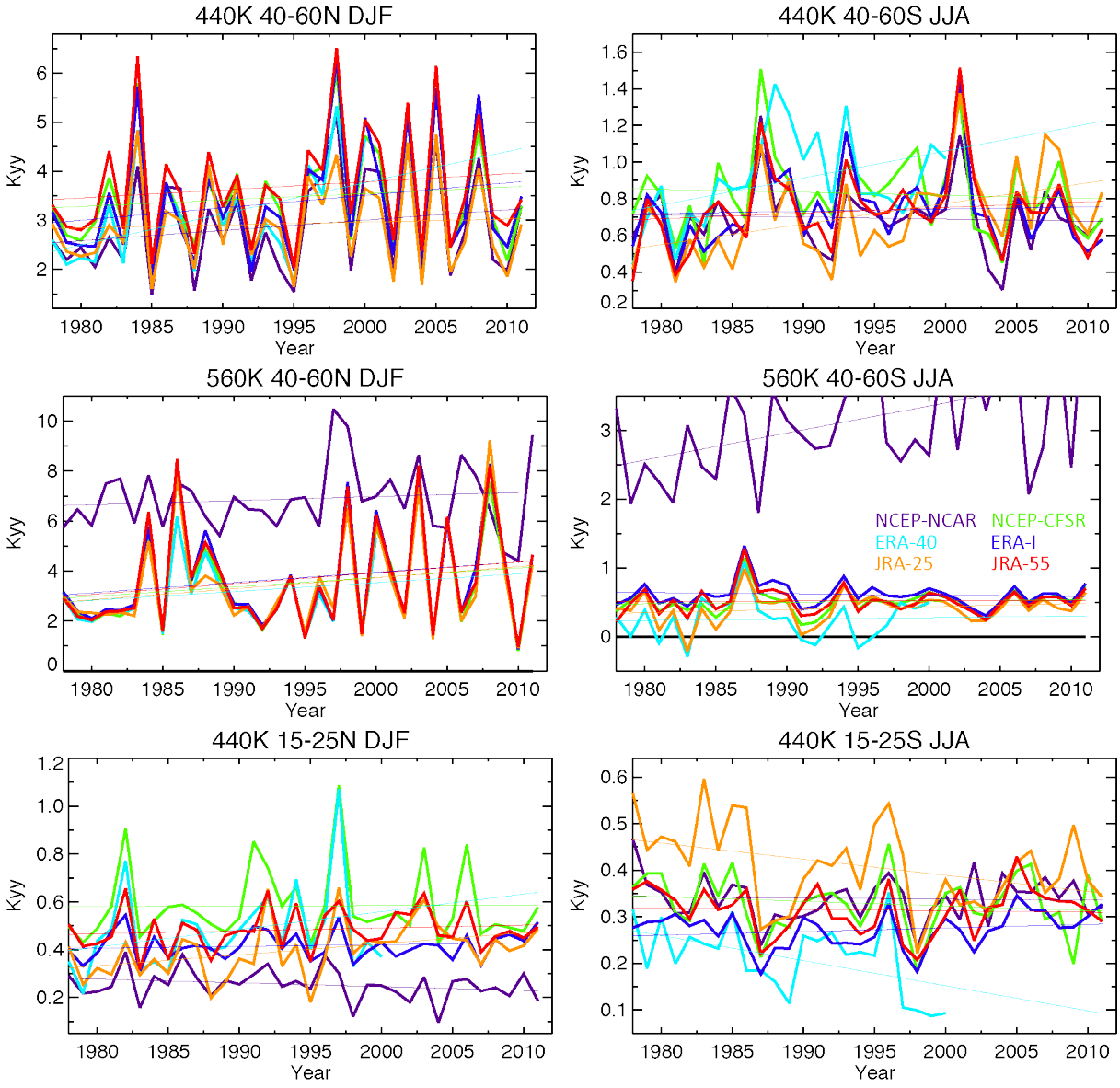

Figure 2. Temporal variations of the isentropic diffusion coefficient Kyy (in 10^6 m^2/s) averaged over 40–60N in DJF (left) and 40–60S in JJA (right) at 440 K (top) and 560 K (bottom) for 1978–2012. The linear trend slope is also shown for each dataset. The results are shown for the NCEP-NCAR reanalysis (purple), NCEP-CFSR (green), ERA-40 (light blue), ERA-Interim (blue), JRA-25 (orange), and JRA-55 (red).

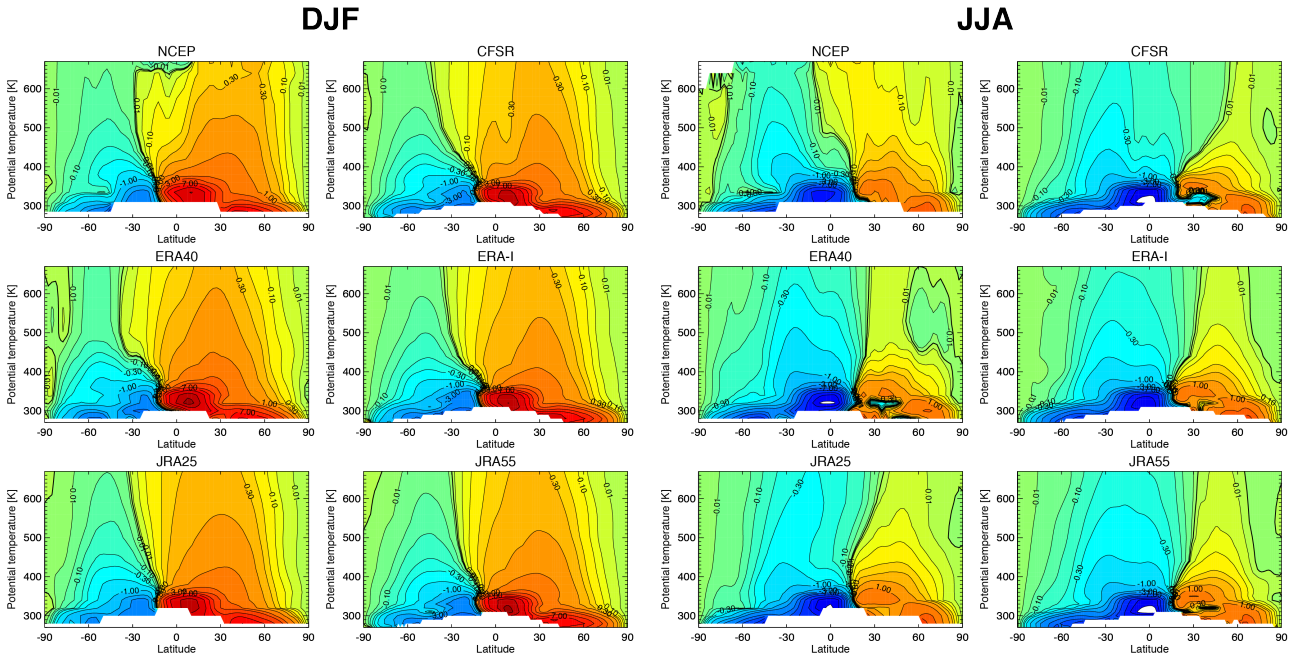

Figure 3. Same as Fig. 1, but for the mass stream function (in 10^{10} kg/s).

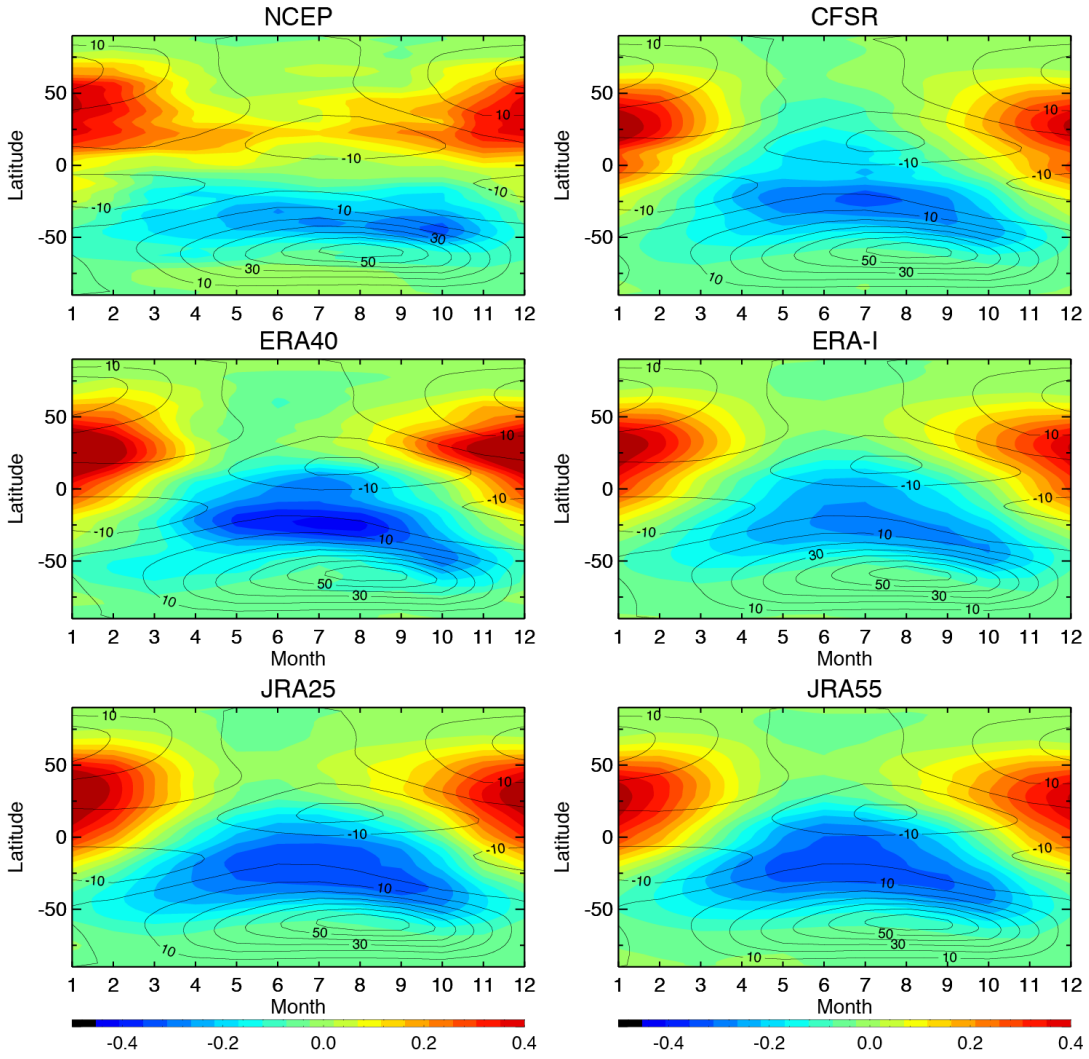

Figure 4. Seasonal variation of the mass stream function (colour contours, in 10^{10} kg/s) and zonal mean zonal wind (black contour lines, with intervals of 10 m/s) at 560 K.

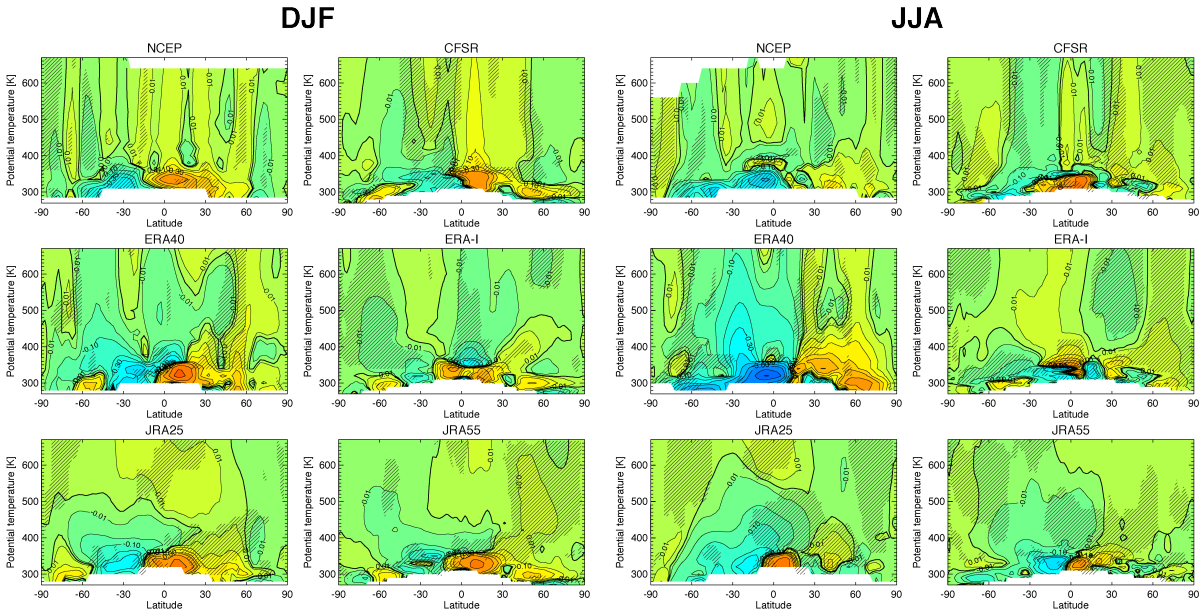

Figure 5. Same as in Fig. 3, but for the linear rend slope (10^{10} kg/s/decade). Statistically significant trends at the 95% level are indicated by hatching

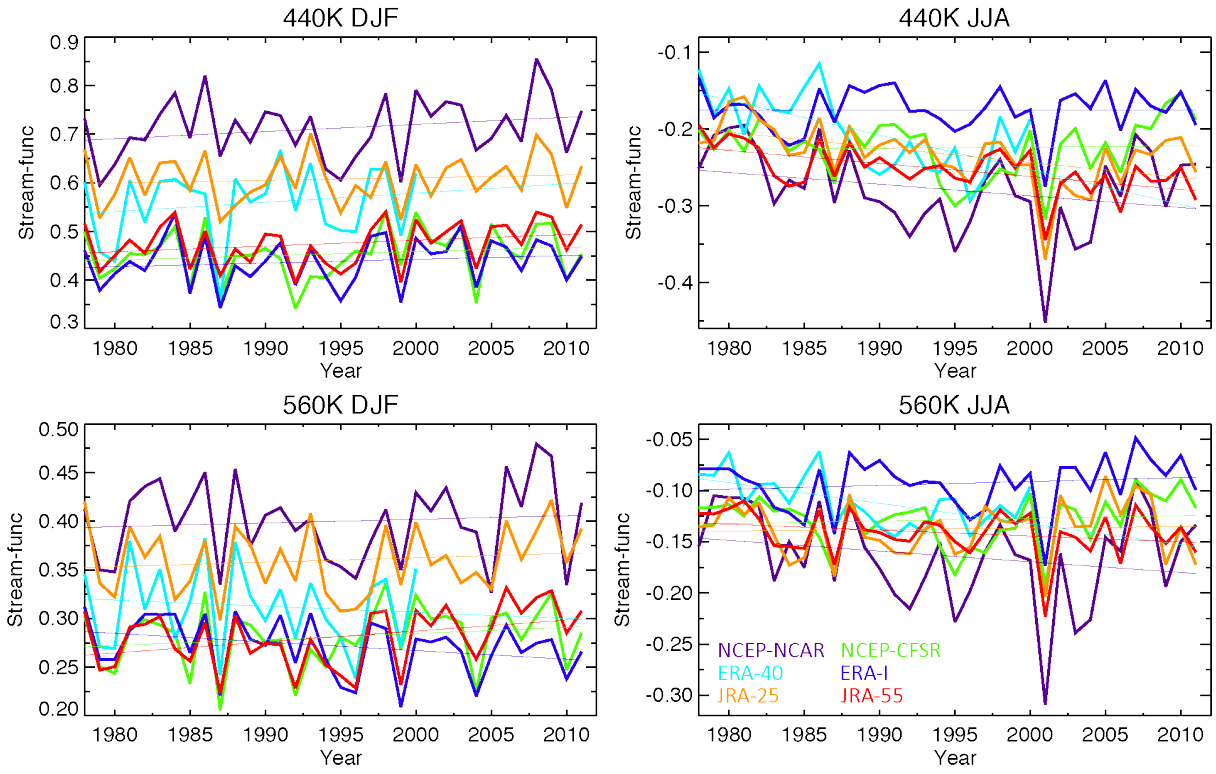

Figure 6. Same as Fig. 2, but for the mass stream function (in 10^{10} kg/s).

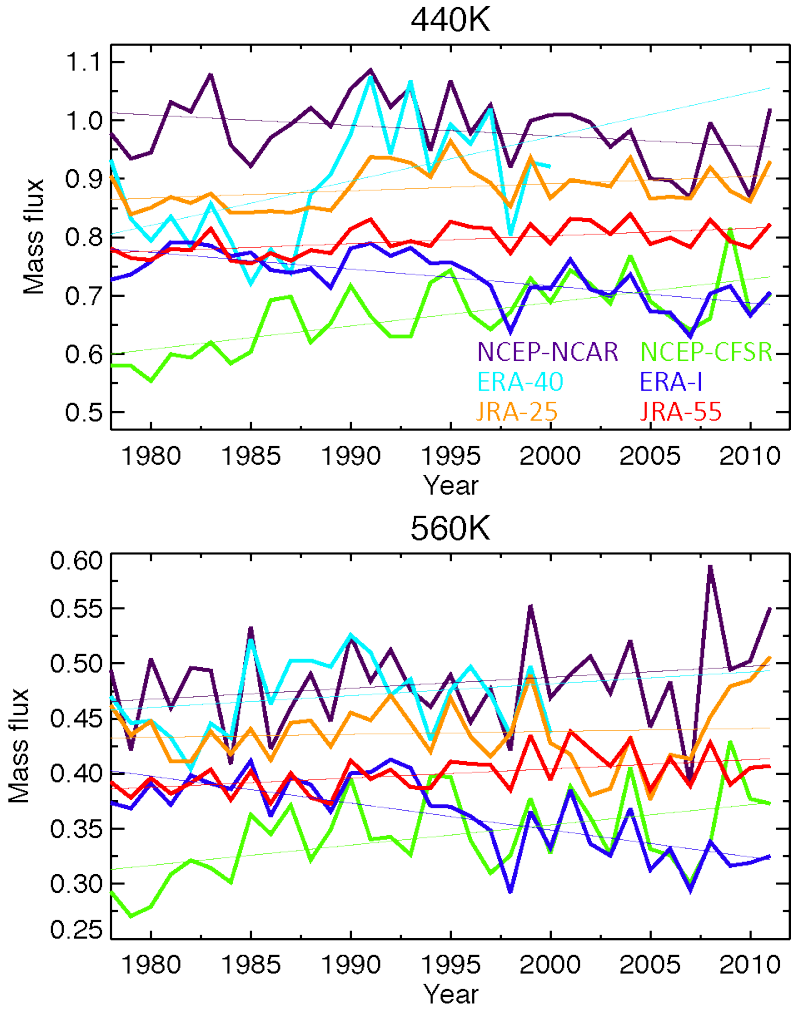

1

2 Figure 7. Temporal variations of the annual mean total mean upward mass flux (in 10^{10} kg/s)
3 at (top) 440 K and (bottom) 560 K.

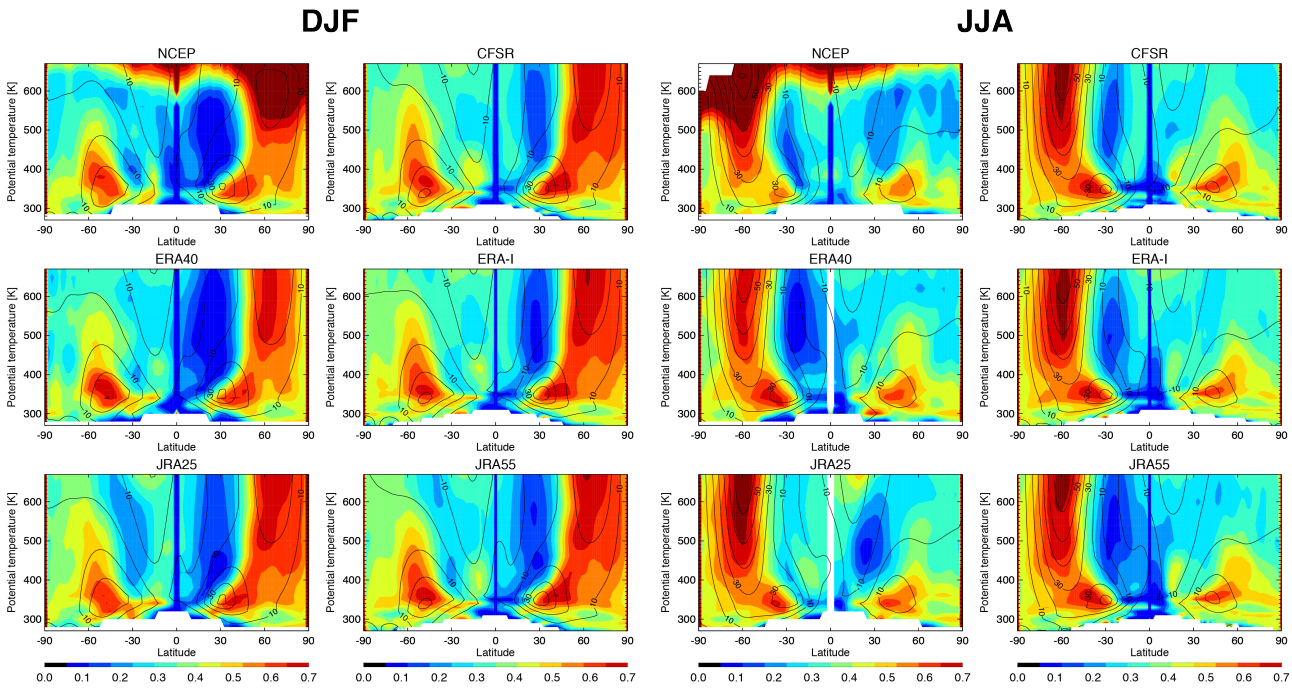

Figure 8. Same as Fig. 1, but for the relative importance of the eddy transport to the total meridional transport. The value larger (smaller) than 0.5 indicates that the eddy transport (mean transport) is dominant in the meridional transport.

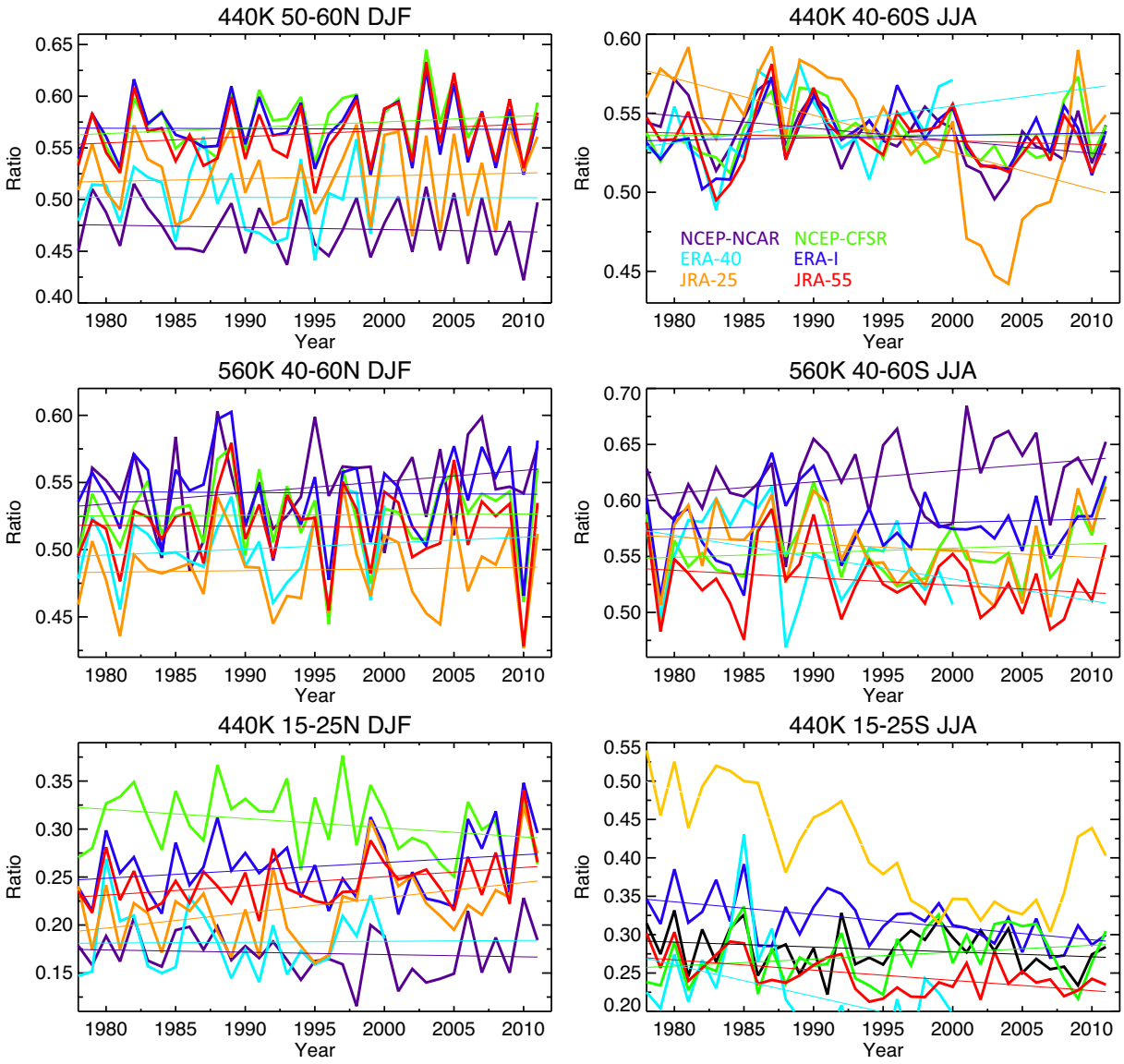

Figure 9. Same as Fig. 2, but for the ratio of the relative importance of the eddy transport to the total meridional transport.

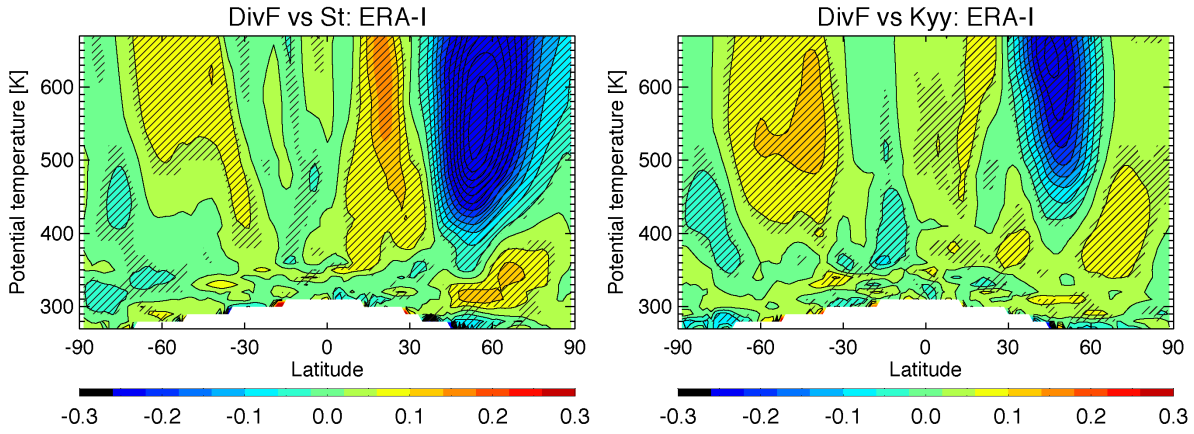

Figure 10. Latitude and potential temperature cross section of the correlation (left) between the mass stream function at 50N, 440 K, and the E–P flux divergence at each grid point, and (right) between Kyy at 50N, 560 K, and the E–P flux divergence at each grid point in DJF in 2000–2012. Correlation coefficients at the 95 % confidence level (following t-test) are indicated by hatching.

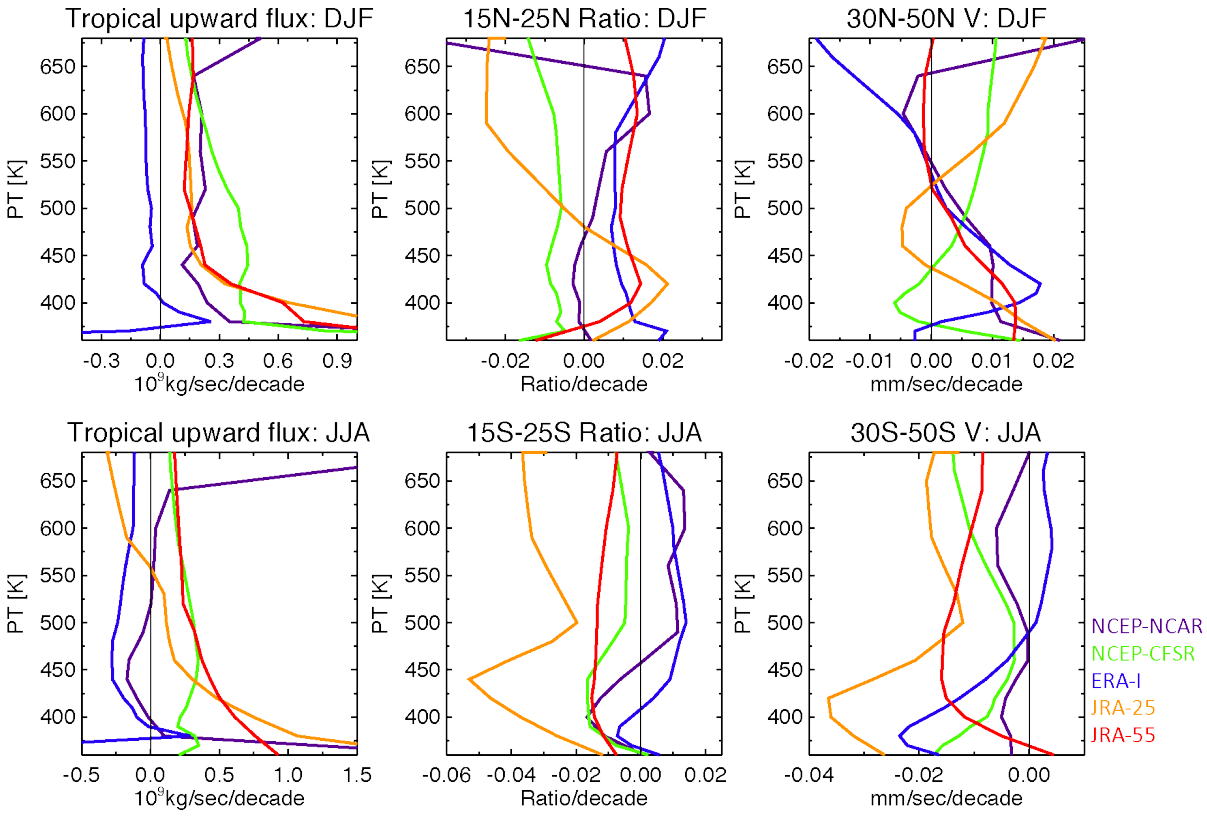

Figure 11. Vertical profiles of the linear trend of the tropical upward mass flux (left, in 10^{10} kg/s/decade), relative contribution of the eddy transport to the total meridional transport

averaged over 15–25° (2nd left, in 1/decade), and the mean meridional velocity $\overline{v^*}$ averaged over 30–50° (m/s/decade) during DJF in the NH (upper panels), and during JJA in the SH (lower panels) for the 34 years, 1979–2012.

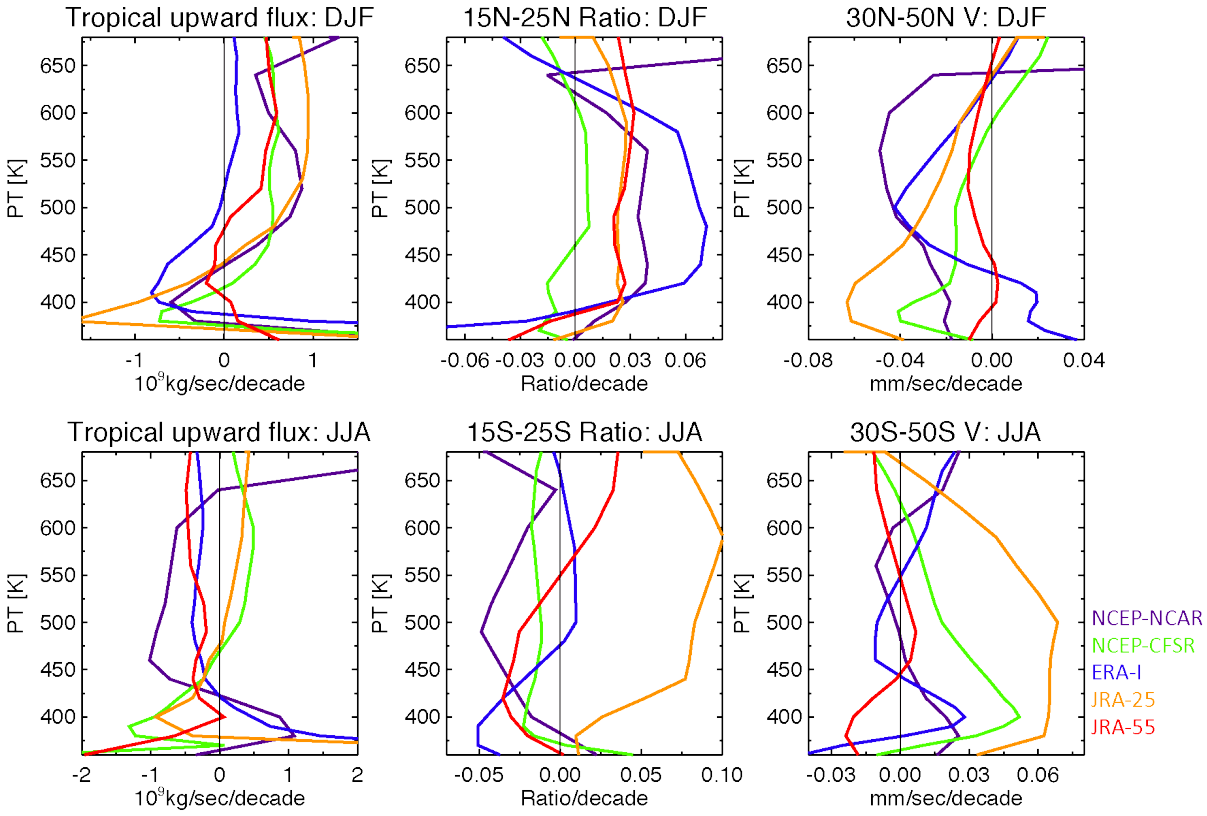

1

2 Figure 12. Same as Fig. 11, but for the last 12 years, 2001–2012.